

Comprehensive full-f drift-kinetic and delta-f gyrokinetic simulations of a linear plasma device based on the gyro-moment approach

J. E. Mencke^{1†}, and P. Ricci¹ and L. Da Silva¹

¹Ecole Polytechnique Fédérale de Lausanne (EPFL), Swiss Plasma Center, CH-1015
Lausanne, Switzerland

(Received xx; revised xx; accepted xx)

First of a kind comprehensive full-f drift-kinetic (DK) and δ -f gyrokinetic (GK) turbulent simulations are carried out in a linear plasma device. We self-consistently derive an electrostatic model including large-scale slowly-varying DK-ordered fields coupled to small-scale rapidly-fluctuating GK-ordered fields. By relying on the critical balance ordering, we show that the electrons are described by a drift-reduced Braginskii model while we rely on a Hermite-Laguerre spectral expansion for describing both the DK and GK parts of the ion distribution function. Global simulations are carried out using the parameters of the linear device LAPD, showing that the DK part of the ion distribution function is approximately a bi-Maxwellian. Fast spectral convergence both for the DK and GK Hermite-Laguerre expansion coefficients is observed, and that the GK fields do not affect the DK fields at the physical LAPD collisionality. Only when the collisionality is reduced and the source term is amplified for the GK fluctuations, an amplification of small-scale turbulent structures is observed. The findings are supported by linear results that show that the simulations are dominated by turbulent fluctuations that are Kelvin-Helmholz driven. Additionally, a GK Kelvin-Helmholz-like mode is observed in the low-GK-collisionality regime which can non-linearly drive small-scale structures.

1. Introduction

Modeling the boundary region of magnetically confined fusion plasmas remains a challenge for the fusion community. Fluctuations at all scales need to be considered, as well as kinetic effects and collisional processes. Developing a model for simulating

† Email address for correspondence: jacob.mencke@epfl.ch

the plasma boundary requires overcoming the limitations of existing models. Full-f fluid codes focus on the long-wavelength limit Paruta *et al.* (2018); Giacomini *et al.* (2022), and their validity is limited to the highly collisional regime. Gyrofluid codes apply Padé approximation to relax the long-wavelength approximation Held & Wiesenberger (2022); Held *et al.* (2020). Additionally, they use kinetic closures to avoid considering the highly collisional limit, although the success of these closures is highly case dependent Beer & Hammett (1996); Wiesenberger & Held (2022, 2023). On the other hand, gyrokinetic (GK) δ -f models, which offer a good description of the core of fusion plasmas Pan *et al.* (2016); Jenko *et al.* (2000), present the challenge of including collisions at the level of relevance for the boundary. Furthermore, their application to the boundary is questionable due to large-scale fluctuations present in this region. Full-f GK codes often focus on the long-wavelength limit Chang *et al.* (2017); Dorf & Dorr (2020); Hakim *et al.* (2020); Michels *et al.* (2022); Ulbl *et al.* (2023) and thus compromise physical fidelity at the cost of computational performance.

To overcome the limitations of these approaches and accurately describe the boundary, Qin *et al.* (2006); Hahm *et al.* (2009); Frei *et al.* (2020), propose a model that couples a DK and GK ordering. Here, we leverage the work of Frei *et al.* (2020) and present a first implementation of a model that couples DK and GK orderings. More precisely, this work relies on splitting the distribution functions into a drift-kinetic (DK) large-scale slowly-varying part and a GK small-scale rapidly-varying part. The DK fields are allowed to be large in amplitude but only vary on long scale, employing a long-wavelength limit, while the GK fields are small in amplitude but allowed to vary on all scales.

The model is based on single particle equations of motion derived from first principles starting from the particle one-form. From the single particle equations of motion, the gyro-averaged Boltzmann equation is derived, split into a GK part and a DK part, and projected onto a Hermite-Laguerre basis giving a DK and a GK hierarchy equation for the projection coefficients, denoted as gyromoments. The Hermite-Laguerre projection allows for an efficient implementation of the plasma dynamics, including multiple different collision operators. Finally, we split the electrostatic potential into a DK part and a GK part, similarly to the distribution functions, and we derive a DK and GK Poisson equation from first-principles by using a variational principle.

Previous δ -f GK gyromoment simulations based on the Hermite-Laguerre projection are shown to efficiently reduce the computational complexity of solving the GK system

of equations compared to continuum δ -f GK simulations Hoffmann *et al.* (2023b,a); Mandell *et al.* (2022). Similarly, full-f gyromoment simulations were performed in a linear plasma device, within a DK ordering Frei *et al.* (2024); Mencke & Ricci (2025). This work combines the advantages of the two previously developed models allowing for order-one DK fluctuations with small wavenumbers and, at the same time, small-amplitude GK fluctuations with arbitrary wavenumbers. It then enables the study of instabilities on all scales while still removing the single-particle gyromotion from the description.

Although our approach ultimately is intended for the boundary of magnetically confined fusion devices, we consider the simpler case of a linear plasma device in this work. A linear plasma device offers an ideal testbed for new global turbulent plasma simulations. The absence of drifts associated with the curvature of the magnetic field, together with the smaller size of the simulations compared to toroidal devices reduces the complexity and cost of the simulations and allows for a deeper understanding of the physics at play Friedman *et al.* (2012). We note that, despite their simple geometries, previous simulations of linear plasma devices show complex turbulent behavior Shi *et al.* (2017); Pan *et al.* (2016, 2018); Popovich *et al.* (2010); Rogers & Ricci (2010); Frei *et al.* (2024); Mencke & Ricci (2025). Finally, the perpendicular incidence of the magnetic field with the walls at the end of the plasma column simplify the boundary conditions of the simulations.

This paper is structured as follows. In section Sec. 2 we present the ordering used as well as the equations describing the evolution of the distribution functions. The DK model for the ions and electrons is derived in Sec. 3 from a kinetic description, and similarly, the GK model is derived in Sec. 4. We close the system in Sec. 5, by deriving the DK and GK Poisson equations used to solve for the two electrostatic potentials. The numerical implementation of the physical model is described in Sec. 6. In Sec. 7 we report the results of the comprehensive turbulent simulations comparing it with a full-f DK simulation where the GK perturbations are suppressed. Section 8 provides an analysis of the findings in Sec. 7 by presenting linear investigations of the turbulence-driving instabilities. Finally, the conclusions follow in Sec. 9.

2. Ordering assumptions and equations of motion

We focus on the case of a fully-ionized plasma with one single-ionized ion species such that the plasma is composed of species $a = i, e$ with e denoting the electrons and i the

only ion species with charge $q_i = e$. We split the electrostatic potential

$$\phi(\mathbf{x}) = \phi_{DK}(\mathbf{x}) + \phi_{GK}(\mathbf{x}), \quad (2.1)$$

where \mathbf{x} is the particle position and we impose that the GK part of the electrostatic potential has a small amplitude compared to the DK part, $\phi_{GK}/\phi_{DK} \sim \epsilon_\delta < 1$. We order the DK and GK quantities such that they vary on different length scales. More precisely, we order the perpendicular gradient lengths, $k_{\perp DK} \sim |\nabla_{\perp} \ln F_{aDK}| \sim |\nabla_{\perp} \ln \phi_{DK}| \sim \epsilon_{\perp}/\rho_s$ with $\epsilon_{\perp} < 1$ and $k_{\perp GK} \sim |\nabla_{\perp} \ln \phi_{GK}| \sim 1/\rho_s$, being $\rho_s = c_s/\Omega_i$ the ion sound Larmor radius with $c_s = \sqrt{T_e/m_i}$ the sound speed, T_e the electron temperature, and $\Omega_i = q_i B/m_i$ the ion gyro frequency, with B the magnetic field strength. Furthermore, we order the parallel length scale as $k_{\parallel} \sim \epsilon k_{\perp DK}$ and the frequency as $\omega \sim \Omega_i \epsilon \epsilon_{\perp}$. This ordering imposes that ϕ_{DK} gives a contribution to the $\mathbf{E} \times \mathbf{B}$ velocity on the order of $\epsilon_{\perp}/\epsilon_\delta$ with respect to that of ϕ_{GK} Frei *et al.* (2020). By further ordering $\epsilon_{\perp} \sim \epsilon_\delta$, we impose that the $\mathbf{E} \times \mathbf{B}$ drift from the DK electrostatic potential contributes to the drifts, comparably to the GK counterpart.

Based on this ordering, we derive the single-particle dynamics in Sec. 2.1. The behavior of the full distribution function is described in Sec. 2.2 using the Boltzmann equation. Finally, the evolution of the DK and GK parts of the distribution function, is derived from the Boltzmann equation in Sec. 2.3.

2.1. Single-particle dynamics

We assume that the collisionless particle dynamics be governed by the gyrocenter single-particle Lagrangian, Γ_A . By using a Lie approach and including all terms up to second order in the GK and DK parts of the $\mathbf{E} \times \mathbf{B}$ drift (i.e., to order $c_s^2 \epsilon_{\perp}^2$ and $c_s^2 \epsilon_\delta^2$), while assuming a straight and constant magnetic field, we have Frei *et al.* (2020)

$$\Gamma_a(\mathbf{R}, \mu, v_{\parallel}, t) = q_a \mathbf{A}_a^* \cdot \dot{\mathbf{R}} - \frac{\mu B}{\Omega_i} \dot{\theta} - m_a v_{\parallel}^2 / 2 - q_a \Phi_a^* + \mathcal{O}\left(\frac{m_a}{m_i} T_a \epsilon_{\perp}^3, \frac{m_a}{m_i} T_a \epsilon_\delta^3\right), \quad (2.2)$$

where $v_{\parallel} = \mathbf{v} \cdot \mathbf{b}$ is the velocity component parallel to the magnetic field, \mathbf{b} being the unit vector in the direction of the magnetic field, $\mu = m_a v_{\perp}^2 / B$ is the adiabatic invariant, m_a is the mass of species a , and $v_{\perp} = |\mathbf{v} - \mathbf{b} v_{\parallel}|$ is the velocity component perpendicular to the magnetic field. We also define the fields $q_a \Phi_a^* = q_a \phi_{DK} + \mu B + q_a \Phi_E + q_a \langle \psi \rangle_{\mathbf{R}}$ and $q_a \mathbf{A}_a^* = q_a \mathbf{A} + m_a v_{\parallel} \mathbf{b} + m_a \mathbf{u}_E$, where $q_a \Phi_E = m_a |\mathbf{u}_E|^2 / 2 + \mu B \nabla_{\perp}^2 \phi_{DK} / (2B \Omega_a)$ and $\mathbf{u}_E = -\nabla \phi_{DK} \times \mathbf{B} / B^2$ is the $\mathbf{E} \times \mathbf{B}$ velocity for the DK potential. The effective GK

gyro-averaged potential is defined as

$$\langle \psi \rangle_{\mathbf{R}} = \langle \phi_{GK} \rangle_{\mathbf{R}} + \frac{q_a^2}{2m_a \Omega_a} \partial_\mu \left(\langle \phi_{GK} \rangle_{\mathbf{R}}^2 - \langle \phi_{GK}^2 \rangle_{\mathbf{R}} \right) + \frac{q_a}{2m_a \Omega_a^2} \left\langle \left(\mathbf{b} \times \nabla \overline{\phi_{GK}} \right) \cdot \nabla \overline{\phi_{GK}} \right\rangle_{\mathbf{R}}, \quad (2.3)$$

where the gyroaverage operator is introduced,

$$\langle f \rangle_{\mathbf{R}} = \frac{1}{2\pi} \int_0^{2\pi} d\theta \int d\mathbf{x} \delta(\mathbf{R} + \rho - \mathbf{x}) f(\mathbf{x}, \mu, v_\parallel, t) \quad (2.4a)$$

$$= \frac{1}{2\pi} \int_0^{2\pi} d\theta \sum_{n=0}^{\infty} \frac{(\boldsymbol{\rho}_a \cdot \nabla)^n}{n!} f(\mathbf{R}, \mu, v_\parallel, t) \quad (2.4b)$$

$$= \sum_{n=0}^{\infty} \left(\frac{2\mu}{q_a \Omega_a} \right)^n \frac{\nabla_\perp^{2n}}{2^n n! n!} f(\mathbf{R}, \mu, v_\parallel, t), \quad (2.4c)$$

with $\delta(\cdot)$ the Dirac delta function and $\boldsymbol{\rho}_a = \mathbf{a}v_\perp/\Omega_a$, the Larmor radius, being \mathbf{a} a unit vector perpendicular to both the magnetic field and the gyromotion of the particle Frei *et al.* (2020). Finally, we define

$$\widetilde{\phi_{GK}} = \phi_{GK} - \langle \phi_{GK} \rangle_{\mathbf{R}}, \quad (2.5a)$$

and

$$\overline{\widetilde{\phi_{GK}}} = \int^\theta d\theta' \widetilde{\phi_{GK}}(\mathbf{x}(\mathbf{R}, \theta'), \mu, v_\parallel, t), \quad (2.5b)$$

in Eq. (2.3).

2.2. Collective behavior

The collective behavior of the distribution function is governed by the gyroaveraged Boltzmann equation Frei *et al.* (2020),

$$\partial_t F_a + \nabla \cdot (\dot{\mathbf{R}} F_a) + \dot{v}_\parallel \partial_{v_\parallel} F_a = \langle S_a \rangle_{\mathbf{R}} + \sum_{b=i,e} \langle C_{ab} \rangle_{\mathbf{R}}, \quad (2.6)$$

where the sources for species a , S_a , are introduced along with the collision operator between species a and b , C_{ab} , the parallel acceleration, \dot{v}_\parallel , and gyrocenter drift, $\dot{\mathbf{R}}$.

The Euler-Lagrange equations of the ion Lagrangian, Eq. (2.2), give

$$v_\parallel = \mathbf{b} \cdot \dot{\mathbf{R}}, \quad (2.7a)$$

$$\dot{\mu} = 0, \quad (2.7b)$$

$$-q_a \mathbf{B}^* \times \dot{\mathbf{R}} - m_a \dot{v}_\parallel \mathbf{b} = q_a \nabla \Phi_a^* + q_a \partial_t \mathbf{A}^*, \quad (2.7c)$$

introducing the effective magnetic field, $\mathbf{B}^* = \nabla \times \mathbf{A}^*$. Now, projecting Eq. (2.7c) on the

\mathbf{B}^* direction and crossing with \mathbf{b} , we obtain respectively

$$\dot{v}_{\parallel} B_{\parallel}^* = -\frac{q_a}{m_a} \mathbf{B}^* \cdot (\nabla \Phi_a^* + \partial_t \mathbf{A}^*), \quad (2.8a)$$

$$\dot{\mathbf{R}} B_{\parallel}^* = \mathbf{B}^* v_{\parallel} + \mathbf{b} \times (\nabla \Phi_a^* + \partial_t \mathbf{A}^*), \quad (2.8b)$$

where $B_{\parallel}^* = \mathbf{B}^* \cdot \mathbf{b}$. Equations (2.8a) and (2.8b) are used to evolve the distribution functions through the Boltzmann equation.

Considering the lowest order in m_e/m_i in Eq. (2.2), the electron one-form becomes

$$\Gamma_e(\mathbf{R}, \mu, v_{\parallel}, t) = q_e \mathbf{A} \cdot \dot{\mathbf{R}} - \frac{\mu B}{\Omega_e} \dot{\theta} - m_e v_{\parallel}^2 / 2 - q_e (\phi_{DK} + \phi_{GK}) + \mathcal{O}\left(\frac{m_e}{m_i} T_a\right), \quad (2.9)$$

with the equations of motion identical to that of the ions in Eq. (2.8), with $B_{\parallel}^* = B$, $m_a = m_e$, $\Phi_e^* = \phi_{DK} + \phi_{GK} - \frac{\mu B}{e}$, $\mathbf{B}^* = \mathbf{B}$, and $\partial_t \mathbf{A}^* = 0$.

2.3. DK and GK Boltzmann equations

Given the equations of motion in Eq. (2.8), Eq. (2.6) can, in principle, be solved with appropriate numerical methods once the sources, S_a , and collision operators, C_{ab} , are defined. However, we rely, in the following, on the splitting of the distribution function in a similar way as ϕ in Eq. (2.1). That is

$$F_a(\mathbf{R}, v_{\parallel}, \mu) = F_{aDK}(\mathbf{R}, v_{\parallel}, \mu) + F_{aGK}(\mathbf{R}, v_{\parallel}, \mu). \quad (2.10)$$

Analogously to the electrostatic potential, we impose, $F_{aGK} \sim \epsilon_{\delta} F_{aDK}$, $|\nabla_{\perp} \ln F_{aDK}| \sim k_{\perp DK}$, and $|\nabla_{\perp} \ln F_{aGK}| \sim k_{\perp GK} \sim 1/\rho_s$.

To separate the DK and GK part of the distribution function, we average Eq. (2.6) over small scales, defining the averaging operator such that for any DK-ordered field, g_{aDK} ,

$$\langle g_{aDK} \rangle_{DK} = g_{aDK}, \quad (2.11a)$$

and for the GK fields

$$\langle F_{aGK} \rangle_{DK} = 0, \quad (2.11b)$$

$$\langle \nabla_{\perp} \langle \phi_{GK} \rangle_{\mathbf{R}} \rangle_{DK} = \nabla_{\perp} \phi_{GK}, \quad (2.11c)$$

$$\langle \nabla_{\parallel} \langle \phi_{GK} \rangle_{\mathbf{R}} \rangle_{DK} = 0, \quad (2.11d)$$

with $\nabla_{\parallel} = \mathbf{b} \cdot \nabla$. The averaging operation removes all fluctuations on the Larmor-radius scale and we assume that only the perpendicular electric field has a large-scale component due to the assumption $\nabla_{\perp} \phi_{DK} \sim \nabla_{\perp} \phi_{GK}$. The leading order (in ϵ_{\perp}) DK average of Eq.

(2.6) is

$$\partial_t F_{aDK} + \nabla \cdot \left(\dot{\mathbf{R}}_{DK} F_{aDK} \right) + \dot{v}_{\parallel DK} \partial_{v_{\parallel}} F_{aDK} = S_{aDK} + \sum_{b=i,e} C_{abDK} + \mathcal{O}(F_a \Omega_i \epsilon \epsilon_{\perp}^2), \quad (2.12a)$$

where

$$\dot{\mathbf{R}}_{DK} = \mathbf{b} v_{\parallel} + \frac{1}{B} \mathbf{b} \times \nabla (\phi_{DK} + \phi_{GK}), \quad \dot{v}_{\parallel DK} = \frac{q_a}{m_a} \nabla_{\parallel} \phi_{DK}, \quad (2.12b)$$

$$S_{aDK} = \langle S_a \rangle_{DK}, \quad C_{abDK} = \langle C_{ab} \rangle_{DK} = C_{ab}(F_{aDK}, F_{bDK}). \quad (2.12c)$$

Finally, the GK Boltzmann equation is retrieved by subtracting Eq. (2.12a) from Eq. (2.6). That is,

$$\begin{aligned} \partial_t F_{aGK} + \nabla \cdot \left(\left(\dot{\mathbf{R}} - \dot{\mathbf{R}}_{DK} \right) F_{aDK} + \dot{\mathbf{R}} F_{GK} \right) + \dot{v}_{\parallel DK} \partial_{v_{\parallel}} F_{aGK} + \dot{v}_{\parallel GK} \partial_{v_{\parallel}} F_{aDK} \\ = \langle S_a \rangle_{\mathbf{R}} - S_{aDK} + \sum_{b=i,e} (\langle C_{ab} \rangle_{\mathbf{R}} - C_{abDK}) + \mathcal{O}(F_a \Omega_i \epsilon \epsilon_{\perp}^2 \epsilon_{\delta}), \end{aligned} \quad (2.13a)$$

with

$$\dot{v}_{\parallel GK} = \frac{q_a}{m_a} \nabla_{\parallel} \langle \phi_{GK} \rangle_{\mathbf{R}}. \quad (2.13b)$$

Eqs. (2.12a) and (2.13a) describe the evolution of the distribution functions given the electrostatic potentials, ϕ_{DK} and ϕ_{GK} .

3. Drift-kinetic governing equations

This section presents the derivation of the part of the model that governs the dynamics of the distribution functions on the DK scale. We simplify the electron evolution described by the DK Boltzmann Eq. (2.12a) using the ordering in Sec. 3.1. Furthermore, also starting from Eq. (2.12a), we derive a gyromoment hierarchy equation for the ions in Sec. 3.2 by expanding the ion distribution function on a Hermite-Laguerre basis.

3.1. Electron drift-kinetic model

For the electrons, we notice that the leading order term in Eq. (2.12a) is order $F_a \Omega_i \epsilon \epsilon_{\perp} \sqrt{m_i/m_e}$. Expanding the electron distribution function in terms of square root of the mass ratio and keeping terms only to first order, $F_{eDK} = F_{eDK0} + F_{eDK1}$, with $F_{eDK1} \sim \epsilon_m F_{eDK0}$ and $\epsilon_m = \sqrt{m_e/m_i}$, the lowest order terms appearing in Eq. (2.12a)

are

$$v_{\parallel} \nabla_{\parallel} F_{eDK0} - \frac{e}{m_e} \nabla_{\parallel} \phi_{DK} \partial_{v_{\parallel}} F_{eDK0} = C_{ee} (F_{eDK0}, F_{eDK0}) + C_{ei} (F_{eDK0}, F_{iDK}), \quad (3.1a)$$

where C_{ei} , at leading order in ϵ_m , is given by (Braginskii (1965))

$$C_{ei} (F_{eDK}, F_{iDK}) = -\frac{L_{ei} N_{eDK}}{8\pi} \partial_{v_{\gamma}} (V_{\beta\gamma} \partial_{v_{\beta}} F_{eDK}) = \mathcal{L}_{ei} (F_{eDK}), \quad (3.1b)$$

with

$$L_{ei} = \frac{3\sqrt{\pi}}{4} \frac{\nu_{ei}}{N_{eDK}} v_{The}^3, \quad v_{The} = \sqrt{\frac{2T_e}{m_e}}, \quad (3.1c)$$

$$V_{\beta\gamma} = \frac{1}{v^3} (v^2 \delta_{\beta\gamma} - v_{\beta} v_{\gamma}). \quad (3.1d)$$

A solution of Eq. (3.1a) is given by

$$F_{eDK0} = N_{e0}(\mathbf{R}, t) \frac{m_e^{3/2}}{(2\pi T_{e0}(\mathbf{R}_{\perp}, t))^{3/2}} \exp\left(-\frac{m_e v^2}{2T_{e0}(\mathbf{R}_{\perp}, t)}\right), \quad (3.2a)$$

$$N_{e0}(\mathbf{R}, t) = N_{e\perp}(\mathbf{R}_{\perp}, t) \exp\left(-\frac{e\phi_{DK}}{T_{e0}(\mathbf{R}_{\perp}, t)}\right). \quad (3.2b)$$

In order to obtain an evolution equation for N_{e0} and T_{e0} , we consider the next order in ϵ_m of the Boltzmann equation, Eq. (2.12a), that is

$$\begin{aligned} \partial_t F_{eDK0} + \frac{1}{B} [\phi_{DK} + \phi_{GK}, F_{eDK0}] + v_{\parallel} \nabla_{\parallel} F_{eDK1} - \frac{e}{m_e} \nabla_{\parallel} \phi_{DK} \partial_{v_{\parallel}} F_{eDK1} \\ = C_{ee}^{(1)} (F_{eDK1}) + \mathcal{L}_{ei} \left(F_{eDK1} - \frac{m_e v_{\parallel} J_{\parallel}}{N_{e0} T_{e0}} F_{e0} \right) + S_{eDK}, \end{aligned} \quad (3.3)$$

with $[f, g] = \mathbf{b} \cdot \nabla f \times \nabla g$. The F_{eDK1} , that solves Eq. (3.3), is

$$F_{eDK1} = \left[\frac{N_{e1}}{N_{e0}} + \frac{P_{e1}}{N_{e0} T_{e0}} \left(\frac{m_e v^2}{2T_{e0}} - \frac{3}{2} \right) \right] F_{eDK0} + f_{sh}, \quad (3.4a)$$

where

$$f_{sh} = \sum_{k=0}^{\infty} v_{\parallel} \frac{F_{eDK}}{N_{e0}} A_k(\mathbf{R}) L_k^{3/2} (m_e v^2 / 2T_{e0}). \quad (3.4b)$$

Truncating f_{sh} at $k = 3$, we determine A_k , as described in App. A, obtaining

$$A_0 = 2 \frac{m_e}{T_{e0}} N_{e0} U_{\parallel eDK}, \quad A_1 = 1.266 C_{P1} + 0.286 \frac{m_e}{T_e} J_{\parallel}, \quad (3.4c)$$

$$A_2 = -0.654 C_{P1} + 0.055 \frac{m_e}{T_e} J_{\parallel}, \quad A_3 = 0.0193 C_{P1} + 0.0238 \frac{m_e}{T_e} J_{\parallel}, \quad (3.4d)$$

being

$$C_{P1} = \frac{1}{T_{e0} \nu_{ee}} \nabla_{\parallel} T_{e1}, \quad \text{and} \quad T_{e1} = \frac{P_{e1}}{N_{e0}}. \quad (3.4e)$$

By taking the moments of Eq. (3.3) with weight 1 and $m_e v^2/2$, we determine an evolution equation for $N_{eDK} = N_{e0} + N_{e1}$ and $T_{eDK} = T_{e0} + T_{e1}$, respectively, that is

$$\partial_t N_{eDK} + \frac{1}{B} [\phi_{DK} + \phi_{GK}, N_{eDK}] + \nabla_{\parallel} (U_{\parallel eDK} N_{eDK}) = S_N + \mathcal{O}(N_e \Omega_i \epsilon \epsilon_{\perp}^3), \quad (3.5a)$$

and

$$\begin{aligned} & \frac{3}{2} \left(\partial_t T_{eDK} + \frac{1}{B} [\phi_{DK} + \phi_{GK}, T_{eDK}] + U_{\parallel eDK} \nabla_{\parallel} T_{eDK} \right) \\ & + T_{eDK} \nabla_{\parallel} U_{\parallel eDK} - \frac{0.71 T_{eDK}}{N_{eDK}} \nabla_{\parallel} J_{\parallel} + \frac{1}{N_{eDK}} \nabla_{\parallel} q_{\parallel er} = \frac{3}{2} S_{Te} + \mathcal{O}(T_e \Omega_i \epsilon \epsilon_{\perp}^3), \end{aligned} \quad (3.5b)$$

being

$$q_{\parallel er} = - \frac{3.16 N_{eDK} T_{eDK}}{m_e \nu_{ee}} \nabla_{\parallel} T_{eDK}, \quad (3.5c)$$

(see App. A for the details of the derivation). We note that Eqs. (3.5a) and (3.5b) correspond to the evolution of the density and electron temperature in the drift-reduced Braginskii model with the electrostatic potential expressed as the sum of the GK and DK electrostatic potentials, $\phi_{DK} + \phi_{GK}$ Braginskii (1965); Zeiler *et al.* (1997); Parra (2019).

3.2. Ion moment hierarchy

For the ions, instead of ordering the ion-ion collision frequency as $\nu_{ii} \ll \omega$ and recover the drift-reduced Braginskii through a similar calculation as in Sec. 3.1, we assume $\nu_{ii} \sim \omega$, similar to Frei *et al.* (2020, 2024); Mencke & Ricci (2025), and expand the DK part of the distribution functions on a Hermite-Laguerre basis

$$F_{iDK}(\mathbf{R}, v_{\parallel}, \mu) = \sum_{p,j=0}^{\infty} \mathcal{N}_{iDK}^{pj}(\mathbf{R}) \frac{H_p(s_{\parallel i}) L_j(x_i)}{\sqrt{2^p p!}} F_{Mi}(s_{\parallel i}, x_i), \quad (3.6a)$$

where we introduce

$$s_{\parallel i} = \frac{v_{\parallel} - U_{\parallel iDK}(\mathbf{R})}{v_{Thi}}, \quad x_i = \frac{\mu B}{T_{i0}}, \quad v_{Thi} = \sqrt{\frac{2T_{i0}}{m_i}}, \quad (3.6b)$$

$$F_{Mi} = \frac{e^{-s_{\parallel i}^2 - x_i}}{(\sqrt{\pi} v_{Thi})^3}, \quad (3.6c)$$

and the background temperature of the ions, T_{i0} , along with the physicists' Hermite polynomials, H_p , and the Laguerre polynomials, L_j . These polynomials satisfy the

following orthogonality relations,

$$\int_{-\infty}^{\infty} dx H_p(x) H_{p'}(x) e^{-x^2} = 2^p p! \delta_{pp'}, \quad (3.7a)$$

$$\int_0^{\infty} dx L_j(x) L_{j'}(x) e^{-x} = \delta_{jj'}, \quad (3.7b)$$

with δ_n^m the Kronecker delta. For simplicity, T_{i0} is chosen as a constant in Eq. (3.6), in contrast to Frei *et al.* (2020) where a dynamical bi-Maxwellian is used as the weight function for the Hermite and Laguerre polynomial basis. We note that the generalization of the projection in Eq. (3.6) onto a basis with anisotropic temperatures is straightforward.

We define the DK velocity-space projection of a general phase-space function, χ , on the p 'th Hermite and j 'th Laguerre polynomial, that is

$$\|\chi\|_i^{pj} = \int_{-\infty}^{\infty} dv_{\parallel} \int_0^{\infty} d\mu \frac{B}{m_i} \int_0^{2\pi} d\theta F_{iDK} \frac{H_p L_j}{\sqrt{2^p p!}} \chi(\mathbf{R}, v_{\parallel}, \mu, \theta). \quad (3.8a)$$

And we further introduce the shorthand notation,

$$\|\chi\|_i = \|\chi\|_i^{00}. \quad (3.8b)$$

We notice that in terms of the projector in Eq. (3.8b) and the gyromoments in Eq. (3.6a), the DK ion density is given by

$$N_{iDK} = \|1\|_i = \mathcal{N}_{iDK}^{00}, \quad (3.9a)$$

the DK ion parallel velocity by

$$U_{\parallel iDK} = \|v_{\parallel}\|_i / N_{iDK}, \quad (3.9b)$$

the DK ion parallel pressure by

$$P_{\parallel iDK} = m_i \left\| (v_{\parallel} - U_{\parallel iDK})^2 \right\|_i = T_{i0} \left(\sqrt{2} \mathcal{N}_{iDK}^{20} + N_{iDK} \right), \quad (3.9c)$$

and the DK ion perpendicular pressure by

$$P_{\perp iDK} = \|\mu B\|_i = T_{i0} (N_{iDK} - \mathcal{N}_{iDK}^{01}). \quad (3.9d)$$

Finally, from Eq. (3.9b), we have that

$$\mathcal{N}_{iDK}^{10} = \sqrt{2} \|s_{\parallel}\|_i = 0. \quad (3.9e)$$

Projecting Eq. (2.12a) for $a = i$ on the Hermite Laguerre basis gives a gyromoment

hierarchy

$$\begin{aligned} & \frac{\partial}{\partial t} \mathcal{N}_{iDK}^{pj} + \frac{\sqrt{2p}}{v_{Thi}} \mathcal{N}_{iDK}^{p-1j} \frac{\partial}{\partial t} U_{\parallel iDK} + \frac{\sqrt{2p}}{v_{Thi}} \left\| \dot{\mathbf{R}} \right\|_{i0}^{p-1j} \cdot \nabla U_{\parallel iDK} \\ & + \nabla \cdot \left\| \dot{\mathbf{R}} \right\|_{i0}^{pj} - \frac{\sqrt{2p}}{v_{Thi}} \left\| \dot{v}_{\parallel} \right\|_{i0}^{p-1j} = \mathcal{C}_{ii0}^{pj} + \mathcal{C}_{ie0}^{pj} + \mathcal{S}_{i0}^{pj}, \end{aligned} \quad (3.10a)$$

with

$$\nabla \cdot \left\| \dot{\mathbf{R}} \right\|_{i0}^{pj} = \nabla_{\parallel} \left\| v_{\parallel} \right\|_i^{pj} + \frac{1}{B} \left[\phi_{DK} + \phi_{GK}, \mathcal{N}_{iDK}^{pj} \right], \quad (3.10b)$$

$$\left\| \dot{\mathbf{R}} \right\|_{i0}^{pj} \cdot \nabla U_{\parallel iDK} = \left\| v_{\parallel} \right\|_i^{pj} \nabla_{\parallel} U_{\parallel iDK} + \frac{\mathcal{N}_{iDK}^{pj}}{B} \left[\phi_{DK} + \phi_{GK}, U_{\parallel iDK} \right], \quad (3.10c)$$

$$\left\| \dot{v}_{\parallel} \right\|_i^{pj} = -\frac{q_i}{m_i} \mathcal{N}_{iDK}^{pj} \nabla_{\parallel} \phi_{DK}, \quad (3.10d)$$

and

$$\left\| v_{\parallel} \right\|_i^{pj} = \frac{v_{Thi}}{\sqrt{2}} \left(\sqrt{p+1} \mathcal{N}_{iDK}^{p+1j} + \sqrt{p} \mathcal{N}_{iDK}^{p-1j} \right) + U_{\parallel iDK} \mathcal{N}_{iDK}^{pj}, \quad (3.10e)$$

where we introduce the small-scale-averaged projection of the ion-ion collision operator, $\mathcal{C}_{ii0}^{pj} = \|C_{iiDK}/F_{iDK}\|^{pj}$, the ion-electron collision operator, $\mathcal{C}_{ie0}^{pj} = \|C_{ieDK}/F_{iDK}\|^{pj}$, and the ion source, $\mathcal{S}_{i0}^{pj} = \|S_{iDK}/F_{iDK}\|^{pj}$.

The equation for $U_{\parallel iDK}$ is retrieved by setting $(p, j) = (1, 0)$ in Eq. (3.10a), that is

$$\begin{aligned} m_i N_{iDK} \partial_t U_{\parallel iDK} &= -m_i N_{iDK} \left(U_{\parallel iDK} \nabla_{\parallel} U_{\parallel iDK} + \frac{1}{B} \left[\phi_{DK} + \phi_{GK}, U_{\parallel iDK} \right] \right) \\ &\quad - \nabla_{\parallel} P_{\parallel iDK} - e \nabla_{\parallel} \phi_{DK} - F_{ei} + \frac{m_i}{\sqrt{2}} v_{Thi} S_{i0}^{10} + \mathcal{O}(m_i N_{iDK} c_s \omega), \end{aligned} \quad (3.11a)$$

with

$$F_{ei} = m_e \int d\mathbf{v} v_{\parallel} C_{ei} = -m_i \int d\mathbf{v} v_{\parallel} C_{ie}, \quad (3.11b)$$

due to conservation of momentum.

Explicitly inserting the relation for $\partial_t U_{\parallel iDK}$, Eq. (3.11a), in Eq. (3.10a) we get

$$\begin{aligned} & \partial_t \mathcal{N}_{iDK}^{pj} + \nabla_{\parallel} \left\| v_{\parallel} \right\|_i^{pj} + \sqrt{p} \left\| s_{\parallel} \right\|_i^{p-1j} \nabla_{\parallel} U_{\parallel iDK} + \frac{1}{B} \left[\phi_{DK} + \phi_{GK}, \mathcal{N}_{iDK}^{pj} \right] \\ & - \frac{\sqrt{2p} \mathcal{N}_{iDK}^{p-1j}}{N_{iDK}} \frac{1}{m_i v_{Thi}} \nabla_{\parallel} P_{\parallel iDK} = \sum_s C_{is}^{pj} + S_{i0}^{pj} - \frac{\sqrt{p} \mathcal{N}_{iDK}^{p-1j}}{N_{iDK} m_i v_{Thi}} S_U, \end{aligned} \quad (3.12a)$$

$$\left\| s_{\parallel} \right\|_i^{pj} = \sqrt{p+1} \mathcal{N}_{iDK}^{p+1j} + \sqrt{p} \mathcal{N}_{iDK}^{p-1j}. \quad (3.12b)$$

Finally, we use a long-wavelength Dougherty collision operator Dougherty (1964) in

Eq. (3.12a) whose projection is given by Frei *et al.* (2024); Mencke & Ricci (2025)

$$\begin{aligned} \mathcal{C}_{ii0}^{pj} = & \nu_i \left[-(p+2j) \mathcal{N}_{iDK}^{pj} + (T_{iDK} - 1) \right. \\ & \left. \times \left(\sqrt{p(p-1)} \mathcal{N}_{iDK}^{p-2j} - 2j \mathcal{N}_{iDK}^{pj-1} \right) \right], \end{aligned} \quad (3.13)$$

with $\nu_i = \nu_0 1.38 \sqrt{m_i/m_e} (T_{iDK}/T_{e0})^{-3/2}$ and $\nu_0 = 4\sqrt{2\pi} e^4 N_0 \sqrt{m_e} \ln \lambda / [3m_i T_{e0}^{3/2} 1.96 (4\pi\epsilon_0)^2]$.

4. Gyrokinetic governing equations

For the governing equations of the GK fields, we first develop the GK part of the electron distribution function in a similar way as the DK counterpart assuming an adiabatic response to the GK electrostatic potential. We then derive a moment hierarchy for the GK ion gyromoments, similarly as for the DK ion gyromoments.

Focusing first on the electron species, we perturbatively solve the Boltzmann equation by expanding in orders of ϵ_m . We first write down the order $\epsilon_m^{-1} \partial_t F_{eGK}$ of Eq. (2.13a) with $a = e$, that is

$$v_{\parallel} \nabla_{\parallel} F_{eGK} - \frac{e}{m_e} \nabla_{\parallel} \phi_{DK} \partial_{v_{\parallel}} F_{eGK} - \frac{e}{m_e} \nabla_{\parallel} \phi_{GK} \partial_{v_{\parallel}} F_{eDK} = \mathcal{C}_{ee1}(F_{eDK}, F_{eGK}) + \mathcal{L}_{ei}(F_{eGK}). \quad (4.1)$$

Since Eq. (4.1) is linear in F_{eGK} , its general solution is given by

$$F_{eGK} = \left(\frac{\delta N_{eGK}(\mathbf{R}_{\perp}, t)}{N_{eDK}} + \frac{e\phi_{GK}}{T_{eDK}} \right) F_{eDK}, \quad (4.2)$$

where δN_{eGK} is a free parameter. We set $\delta N_{eGK} = 0$, allowing us to close our system of equations. This corresponds to an adiabatic Boltzmann response for the GK part of the electron distribution function.

For the ions, similarly to the DK system, we expand the GK part of the ion distribution function on a Hermite-Laguerre basis

$$F_{iGK}(\mathbf{R}, v_{\parallel}, \mu) = \sum_{p,j=0}^{\infty} \mathcal{N}_{iGK}^{pj}(\mathbf{R}) \frac{H_p(s_{\parallel i}) L_j(x_i)}{\sqrt{2^p p!}} F_{Mi}(s_{\parallel i}, x_i). \quad (4.3a)$$

The GK velocity-space projection of a general phase-space function, χ , is defined

$$\|\chi\|_i^{\delta pj} = \int_{-\infty}^{\infty} dv_{\parallel} \int_0^{\infty} d\mu \frac{B}{m_i} \int_0^{2\pi} d\theta F_{iGK} \frac{H_p L_j}{\sqrt{2^p p!}} \chi(\mathbf{R}, v_{\parallel}, \mu, \theta), \quad (4.3b)$$

where we additionally define,

$$\|\chi\|_i^{\delta} = \|\chi\|_i^{\delta 00}. \quad (4.3c)$$

The first few moments of the GK distribution function can be expanded in terms of the GK and DK fluid quantities and gyromoments as follows

$$\|1\|_i^\delta = \mathcal{N}_{iGK}^{00} = N_{iGK}, \quad (4.3d)$$

$$\|v_{\parallel}\|_i^\delta = U_{\parallel iDK} N_{iGK} + \frac{v_{Thi}}{\sqrt{2}} \mathcal{N}_{iGK}^{10} = N_{iDK} U_{\parallel iGK} + U_{\parallel iDK} N_{iGK}, \quad (4.3e)$$

$$\begin{aligned} m_i \left\| (v_{\parallel} - U_{\parallel iDK})^2 \right\|_i^\delta - 2m_i \left\| (v_{\parallel} - U_{\parallel iDK}) U_{\parallel iGK} \right\|_i \\ = T_{i0} \left(\sqrt{2} \mathcal{N}_{iGK}^{20} + N_{iGK} \right) = P_{\parallel iGK}, \end{aligned} \quad (4.3f)$$

$$\|\mu B\|_i^\delta = T_{i0} (N_{iGK} - \mathcal{N}_{iGK}^{01}) = P_{\perp iGK}, \quad (4.3g)$$

and, from Eq. (4.3e), it follows that

$$U_{\parallel iGK} = \frac{v_{Thi}}{\sqrt{2}} \frac{\mathcal{N}_{iGK}^{10}}{N_{iDK}}. \quad (4.3h)$$

In order to derive the evolution equations for \mathcal{N}_{iGK}^{pj} , we project Eq. (2.13a) with $a = i$ on the Hermite-Laguerre basis, thus obtaining

$$\begin{aligned} \frac{\partial}{\partial t} \mathcal{N}_{iGK}^{pj} + \frac{\sqrt{2p}}{v_{Thi}} \left\| \dot{\mathbf{R}} \right\|_{i1}^{p-1j} \cdot \nabla U_{\parallel iDK} + \nabla \cdot \left\| \dot{\mathbf{R}} \right\|_{i1}^{pj} - \frac{\sqrt{2p}}{v_{Thi}} \|\dot{v}_{\parallel}\|_{i1}^{p-1j} \\ + \frac{\sqrt{2p}}{v_{Thi}} \mathcal{N}_{iGK}^{p-1j} \frac{\partial}{\partial t} U_{\parallel iDK} + \frac{\sqrt{2p}}{v_{Thi}} \left\| \dot{\mathbf{R}} \right\|_{i1}^{\delta p-1j} \cdot \nabla U_{\parallel iDK} + \nabla \cdot \left\| \dot{\mathbf{R}} \right\|_{i1}^{\delta pj} - \frac{\sqrt{2p}}{v_{Thi}} \|\dot{v}_{\parallel}\|_{i1}^{\delta p-1j} \\ = \mathcal{C}_{ii1}^{pj} + \mathcal{C}_{ie1}^{pj} + \delta S_i^{pj}, \end{aligned} \quad (4.4a)$$

where

$$\left\| \dot{\mathbf{R}} \right\|_{i1}^{pj} \cdot \nabla U_{\parallel} = \frac{1}{B} \|\mathbf{b} \times \nabla (\langle \psi \rangle_{\mathbf{R}} - \langle \phi_{GK} \rangle_{\mathbf{R}})\|_i^{pj} \cdot \nabla U_{\parallel} + \frac{1}{B} \|\mathbf{b} \times \nabla \langle \widetilde{\phi_{GK}} \rangle_{\mathbf{R}}\|_i^{pj} \cdot \nabla U_{\parallel}, \quad (4.4b)$$

$$\nabla \cdot \left\| \dot{\mathbf{R}} \right\|_{i1}^{pj} = \frac{1}{B} \nabla \cdot \|\mathbf{b} \times \nabla (\langle \psi \rangle_{\mathbf{R}} - \langle \phi_{GK} \rangle_{\mathbf{R}})\|_i^{pj} + \frac{1}{B} \nabla \cdot \|\mathbf{b} \times \nabla \langle \widetilde{\phi_{GK}} \rangle_{\mathbf{R}}\|_i^{pj}, \quad (4.4c)$$

$$\|\dot{v}_{\parallel}\|_{i1}^{pj} = -\frac{q_i}{m_i} \|\nabla_{\parallel} \langle \phi_{GK} \rangle_{\mathbf{R}}\|_i^{pj}, \quad (4.4d)$$

$$\begin{aligned} \mathcal{N}_{iGK}^{p-1j} \frac{\partial}{\partial t} U_{\parallel} + \left\| \dot{\mathbf{R}} \right\|_{i1}^{\delta p-1j} \cdot \nabla U_{\parallel} - \|\dot{v}_{\parallel}\|_{i1}^{\delta p-1j} = \frac{v_{Thi}}{\sqrt{2}} \|s_{\parallel i}\|_i^{\delta p-1j} \nabla_{\parallel} U_{\parallel} \\ - \frac{\mathcal{N}_{iGK}^{p-1j}}{N_{iDK}} \left(\frac{1}{m_i} \nabla_{\parallel} P_{\parallel i} - \frac{S_U}{m_i} \right), \end{aligned} \quad (4.4e)$$

and

$$\nabla \cdot \left\| \dot{\mathbf{R}} \right\|_{i1}^{\delta pj} = \nabla_{\parallel} \|v_{\parallel}\|_i^{\delta pj} + \frac{1}{B} [\phi_{DK}, \mathcal{N}_{iGK}^{pj}] + \frac{1}{B} \nabla \cdot \|\mathbf{b} \times \nabla \langle \phi_{GK} \rangle_{\mathbf{R}}\|_i^{\delta pj}. \quad (4.4f)$$

In Eq. (4.4a) we introduce the linearized (around F_{iDK} and F_{eDK}) ion-ion and ion-electron collision operator, \mathcal{C}_{ii1}^{pj} and \mathcal{C}_{ie1}^{pj} , and the small-scale source term, $\delta S_1^{pj} =$

$\int d\mathbf{v} H^{pj} (S_i - \langle S_i \rangle_{DK})$. The expressions of the projection of the gyroaveraged quantities involving $\langle \psi \rangle_{\mathbf{R}}$ and $\langle \phi_{GK} \rangle_{\mathbf{R}}$ are reported in App. B. We use the GK Dougherty collision operator in Eq. (4.4a) Frei *et al.* (2020)

$$\begin{aligned} \mathcal{C}_{ii1}^{pj} = & \nu_{i0} \left[-(p+2j) \mathcal{N}_{iGK}^{pj} + \tau_i T_{iDK} \nabla_{\perp}^2 \mathcal{N}_{iGK}^{pj} + (T_{iDK} - 1) \right. \\ & \left. \times \left(\sqrt{p(p-1)} \mathcal{N}_{iGK}^{p-2j} - 2j \mathcal{N}_{iGK}^{pj-1} \right) \right], \end{aligned} \quad (4.5)$$

where we approximate $T_i = T_{iDK}$.

5. Field equations

In order to close our system of equations, we now determine the governing equations for ϕ_{DK} and ϕ_{GK} . In the process, we will also determine a relation between N_{iDK} and N_{eDK} which allows us to avoid solving both Eq. (3.5a) and Eq. (3.12a) with $(p, j) = (0, 0)$. For this purpose, we perform the variation of the action,

$$A = \sum_a \int dt \int d\mathbf{x} \int d\mathbf{v} F_a \Gamma_a, \quad (5.1)$$

with respect to ϕ_{GK} where quasineutrality is imposed by neglecting the field functional action term Frei *et al.* (2020), and Γ_i and Γ_e are defined in Eqs (2.2) and (2.9), respectively. We note that, the variation with respect to ϕ_{DK} , yields an identical result in the long wavelength limit, being accurate only to order $(\rho_s k_{\perp GK})^2$ since we only allow ϕ_{DK} to vary on long scales.

The variation of the action, Eq. (5.1), with respect to ϕ_{GK} gives the following Poisson equation,

$$\begin{aligned} \frac{B_{\parallel}^*}{B} N_{iDK} - N_{eDK} + \frac{1}{2m_i \Omega_i^2} \nabla_{\perp}^2 P_{\perp iDK} + \varrho_i^* - N_{eGK} \\ + \nabla_{GK} (\langle \phi_{GK} \rangle_{\mathbf{R}}) = \mathcal{O} (n_e \epsilon_{\perp}^3, n_e \epsilon_{\delta} \epsilon_{\perp}, n_e \epsilon_{\delta}^2), \end{aligned} \quad (5.2a)$$

where we introduce the GK Poisson operator

$$\nabla_{GK} (\langle \phi_{GK} \rangle_{\mathbf{R}}) = 2\pi \int_{-\infty}^{\infty} dv_{\parallel} \int_0^{\infty} d\mu \frac{B}{m_i} \left(F_{iDK} \frac{e}{B} \partial_{\mu} \langle \phi_{GK} \rangle_{\mathbf{R}}^{\dagger} \right), \quad (5.2b)$$

and the ion GK particle density

$$\varrho_i^* = 2\pi \int_{-\infty}^{\infty} dv_{\parallel} \int_0^{\infty} d\mu \frac{B}{m_i} \langle F_{iGK} \rangle_{\mathbf{x}}^{\dagger}, \quad (5.2c)$$

$$(5.2d)$$

and where the adjoint gyroaverage operator has been defined as

$$\langle f \rangle_{\mathbf{x}}^{\dagger} = \frac{1}{2\pi} \int_0^{2\pi} d\theta \int d\mathbf{R} \delta(\mathbf{R} + \boldsymbol{\rho} - \mathbf{x}) f(\mathbf{R}, \mu, v_{\parallel}, t) \quad (5.3a)$$

$$= \sum_{n=0}^{\infty} \left(\frac{2\mu}{q_a \Omega_a} \right)^n \frac{\nabla_{\perp}^{2n}}{2^n (n!)^2} f(\mathbf{x}, \mu, v_{\parallel}, t), \quad (5.3b)$$

valid for constant B (in this case the gyroaverage operator is self-adjoint).

We impose that Eq. (5.2a) is satisfied independently order by order, up to leading order in ϵ_{\perp} and ϵ_{δ} . For this purpose, we introduce the higher order DK densities such that

$$N_{aDK} = N_{aDK0} + N_{aDK1}, \quad (5.4)$$

with $N_{aDK1} \sim \epsilon_{\perp}^2 N_{aDK}$. This expansion removes the need of evaluating the Pfirsch-Kaufman polarization Pfirsch & Morrison (1985); Kaufman (1986); Frei *et al.* (2020). At order N_e , Eq. (5.2a) reads

$$N_{iDK0} - N_{eDK0} = 0, \quad (5.5)$$

thus we impose $N_{iDK0} = N_{eDK0} = N_{DK}$. By taking the time derivative of Eq. (5.5), using Eq. (3.5a) and Eq. (3.10a) with $(p, j) = (0, 0)$, we relate the electron and ion parallel velocities as follows

$$\nabla_{\parallel} \int dv v_{\parallel} (F_{iDK} - F_{eDK}) \equiv \nabla_{\parallel} J_{\parallel} = \mathcal{O}(n_e \Omega_i \epsilon_{\perp}^3). \quad (5.6)$$

In order to satisfy Eq. (5.6), we assume $J_{\parallel} = \mathcal{O}(c_s n_e \epsilon_{\perp}^2)$. This means that to the lowest order in ϵ_{\perp} , the electrons and ions move with one fluid velocity, U_{\parallel} . Therefore, we define

$$m_i N_{DK} U_{\parallel} \equiv 2\pi \int_{-\infty}^{\infty} dv_{\parallel} \int_0^{\infty} d\mu \frac{B}{m_i} v_{\parallel} (m_e F_{eDK} + m_i F_{iDK}) + \mathcal{O}(c_s \epsilon_{\perp}^2). \quad (5.7)$$

We use that to the lowest order in ϵ_m , $U_{\parallel iDK} = U_{\parallel eDK} + \mathcal{O}(c_s \epsilon_{\perp}^2, c_s \epsilon_m^2)$ and we determine the governing equation for U_{\parallel} as a total momentum equation, adding $m_e N_{DK} \partial_t U_{\parallel eDK} + m_i N_{DK} \partial_t U_{\parallel iDK}$, as it is done in the drift-reduced Braginskii model Braginskii (1965); Zeiler *et al.* (1997); Parra (2019). The moment with $m_e v_{\parallel}$ of Eq. (3.3) gives

$$\begin{aligned} m_e N_{DK} \partial_t U_{\parallel eDK} &= e N_{DK} \nabla_{\parallel} \phi_{DK} - \nabla_{\parallel} P_{eDK} + F_{ei} + \frac{m_e}{\sqrt{2}} v_{The} S_{e0}^{10} \\ &+ \mathcal{O}(m_i N_{DK} c_s \Omega_i \epsilon_{\perp}^3, m_e N_{DK} c_s \Omega_i \epsilon_{\perp}), \end{aligned} \quad (5.8a)$$

and combining Eqs. (3.11a) and (5.8a) gives

$$m_i N_{DK} \left(\partial_t U_{\parallel} + U_{\parallel} \nabla_{\parallel} U_{\parallel} + \frac{1}{B} [\phi_{DK} + \phi_{GK}, U_{\parallel}] \right) + \nabla_{\parallel} P_{\parallel i DK} + \nabla_{\parallel} P_{\parallel e DK} = S_U + \mathcal{O}(m_i N_{DK} c_s \Omega_i \epsilon_{\perp}^3, m_e N_{DK} c_s \Omega_i \epsilon_{\perp}). \quad (5.8b)$$

Thus $\partial_t U_{\parallel}$ is independent of the collision frequencies and we avoid to numerically satisfy momentum conservation, $m_e \int d\mathbf{v}_{\parallel} C_{ei}^{10} = -m_i \int d\mathbf{v}_{\parallel} C_{ie}^{10}$, at high collisionality. In Eq. (5.8b), we define

$$S_U = \frac{1}{\sqrt{2}} (m_i v_{Thi} S_{i0}^{10} + m_e v_{The} S_{e0}^{10}). \quad (5.9)$$

We evolve U_{\parallel} through Eq. (5.8b) and impose $U_{\parallel i} = U_{\parallel e} = U_{\parallel}$ in Eqs. (3.5a), (3.5b), and (3.12a) in our simulations. Furthermore, Eq. (3.5a) is identical to Eq. (3.12a) with $(p, j) = (0, 0)$ so we only evolve Eq. (3.5a) and impose $\mathcal{N}_{iDK}^{00} = N_{eDK} = N_{DK}$. Finally, as an aside, we note that the implicit condition $J_{\parallel} = \mathcal{O}(n_e c_s \epsilon_{\perp}^2, n_e c_s \epsilon_m^2)$ implies parallel force balance given as

$$\frac{e}{m_e} \nabla_{\parallel} \phi_{DK} - \frac{1}{m_e} \nabla_{\parallel} P_{eDK} + \frac{v_{The}}{\sqrt{2}} S_{e0}^{10} - \frac{1}{m_e} F_{ei} - \frac{v_{Thi}}{\sqrt{2}} S_{i0}^{10} + \frac{1}{m_i} \nabla_{\parallel} P_{\parallel i DK} = \mathcal{O}(N_{DK} c_s \Omega_i \epsilon_{\perp}^3, N_{DK} c_s \Omega_i \epsilon_{\perp} \epsilon_m^2). \quad (5.10)$$

In other words, in order for quasi-neutrality to be satisfied to a certain order in ϵ_{\perp} , the acceleration of ions and electrons must balance to the same order.

To obtain an equation for ϕ_{DK} , we have to consider the order ϵ_{\perp}^2 terms of Eq. (5.2a), that is

$$N_{eDK1} - N_{iDK1} = \frac{1}{B\Omega_i} N_{DK} \nabla_{\perp}^2 \phi_{DK} + \frac{1}{2m_i \Omega_i^2} \nabla_{\perp}^2 P_{\perp i DK}. \quad (5.11)$$

In order to avoid a closure problem in ϵ_{\perp} , which arises by evolving N_{eDK1} and N_{iDK1} independently, we define the vorticity,

$$\Omega \equiv N_{eDK1} - N_{iDK1} + \frac{1}{B\Omega_i} \nabla_{\perp} N_{DK} \cdot \nabla_{\perp} \phi_{DK} + \frac{1}{2m_i \Omega_i^2} \nabla_{\perp}^2 P_{\perp i DK} \quad (5.12)$$

as is custom in fluid approaches Zeiler *et al.* (1997). Using Eq. (5.11), Ω can also be written as

$$\Omega = \frac{1}{B\Omega_i} \nabla \cdot \left(N_{DK} \nabla_{\perp} \phi_{DK} + \frac{1}{q_i \Omega_i} \nabla_{\perp} P_{\perp i DK} \right). \quad (5.13)$$

The addition of the pressure contribution in Eq. (5.12) makes Ω independent of collisions. Indeed, the particle density is independent of collision such that $\partial_t n_i$ with

$$n_i \equiv 2\pi \int_{-\infty}^{\infty} dv_{\parallel} \int_0^{\infty} d\mu \frac{B}{m_i} \langle F_{iDK} \rangle_{\mathbf{x}}^{\dagger} = N_{DK} + N_{iDK1} + \frac{1}{2m_i \Omega_i^2} \nabla_{\perp}^2 P_{\perp i DK} + \mathcal{O}(N_{DK} \epsilon_{\perp}^4)$$

is independent of collisions, but not $\partial_t N_{iDK1}$ on its own.

We differentiate each term of Eq. (5.12) with respect to t . For this purpose, we note that, by using the Boltzmann equation, Eq. (2.6), averaged over small-scale fluctuations but including $\epsilon\epsilon_\perp^3$ terms, we have

$$\begin{aligned}
\partial_t N_{iDK1} = & -\nabla_\parallel (U_\parallel N_{iDK1} + N_{DK} U_{i\parallel DK1}) - \frac{1}{B} [\phi_{DK} + \phi_{GK}, \mathcal{N}_{iDK1}] \\
& - \frac{1}{B} [\phi_{DK1} + \phi_{GK1}, \mathcal{N}_{DK}] + S_{N1} + \frac{1}{B\Omega_i} S_N \nabla_\perp^2 \phi_{DK} - \frac{1}{B\Omega_i} \partial_t (N_{DK} \nabla_\perp^2 \phi_{DK}) \\
& + \frac{1}{B^2 \Omega_i} \nabla_\perp \cdot (N_{DK} \nabla_\perp \partial_t \phi_{DK}) - \frac{1}{B\Omega_i} \nabla_\perp^2 \phi_{DK} \nabla_\parallel (N_{DK} U_\parallel) \\
& - \frac{m_i}{2B^3} [|\nabla_\perp \phi_{DK}|^2, N_{DK}] - \frac{1}{2m_i \Omega_i^2 B} [\nabla_\perp^2 \phi_{DK}, P_{\perp iDK}] \\
& + \frac{1}{B\Omega_i} \nabla_\parallel \nabla_\perp \phi_{DK} \cdot \nabla_\perp (\mathcal{N}_{DK} U_\parallel) + \frac{1}{2m_i \Omega_i^2} \nabla_\perp^2 \|\mu B (S_i + C_{ii}) / F_{iDK}\|,
\end{aligned} \tag{5.14a}$$

where the 1 subscript indicates order ϵ_\perp^2 corrections. The last term in Eq. (5.14a) comes from the sources and collisions acting on the particle position and not gyrocenter position. For the time derivative of the higher order electron density, we get

$$\begin{aligned}
\partial_t N_{eDK1} = & -\nabla_\parallel (U_\parallel N_{eDK1} + N_{DK} U_{e\parallel DK1}) - \frac{1}{B} [\phi_{DK} + \phi_{GK}, \mathcal{N}_{iDK1}] \\
& - \frac{1}{B} [\phi_{DK1} + \phi_{GK1}, \mathcal{N}_{DK}] + S_{N1},
\end{aligned} \tag{5.14b}$$

using Eq. (3.12a) and Eq. (3.9d), the time derivative of the pressure term in Eq. (5.12) is given by

$$\begin{aligned}
\partial_t \nabla_\perp^2 P_{\perp iDK} = & -\nabla_\parallel \nabla_\perp^2 (P_{\perp iDK} U_\parallel + Q_{\perp iDK}) \\
& - \frac{1}{B} \nabla_\perp^2 [\phi_{DK} + \phi_{GK}, P_{\perp iDK}] + \nabla_\perp^2 \|\mu B (S_i + C_{ii}) / F_{iDK}\|,
\end{aligned} \tag{5.14c}$$

with $Q_{\perp iDK} = \|v_{\parallel} \mu B\|_i = -v_{Thi} T_{i0} \mathcal{N}_{iDK}^{11} / \sqrt{2}$. Adding Eqs. (5.14a), (5.14b), and (5.14c) while using Eq. (5.12), we notice that all terms including a time derivative combine to $\nabla \cdot (\partial_t N_{DK} \nabla_{\perp} \phi_{DK})$. Finally, using Eq. (3.5a), we get

$$\begin{aligned}
\partial_t \Omega &= \nabla_{\parallel} \left(J_{\parallel} - (N_{eDK1} - N_{iDK1}) U_{\parallel} - \frac{1}{2m_i \Omega_i^2} \nabla_{\perp}^2 (P_{\perp iDK} U_{\parallel} + Q_{\perp iDK}) \right) \\
&\quad - \frac{1}{B} [\phi_{DK} + \phi_{GK}, N_{eDK1} - N_{iDK1}] - \frac{1}{2m_i \Omega_i^2 B} \nabla_{\perp}^2 [\phi_{DK} + \phi_{GK}, P_{\perp iDK}] \\
&\quad - \frac{1}{B \Omega_i} \nabla_{\perp} \cdot \left[\nabla_{\perp} \phi_{DK} \left(\nabla_{\parallel} (U_{\parallel} N_{DK}) + \frac{1}{B} [\phi_{DK} + \phi_{GK}, N_{DK}] - S_N \right) \right] \\
&\quad + \frac{1}{B \Omega_i} \nabla_{\perp} \partial_t \phi_{DK} \cdot \nabla_{\perp} N_{DK} + \frac{m_i}{2B^3} [|\nabla_{\perp} \phi_{DK}|^2, N_{DK}] \\
&\quad - \frac{1}{2m_i \Omega_i^2 B} [\nabla_{\perp}^2 \phi_{DK}, P_{\perp iDK}] - \frac{1}{B \Omega_i} \nabla_{\perp} \cdot (N_{DK} \nabla_{\perp} \partial_t \phi_{DK}) \\
&\quad + \frac{1}{B \Omega_i} (N_{DK} \nabla_{\perp}^2 \partial_t \phi_{DK}) + \frac{1}{B \Omega_i} S_N \nabla_{\perp}^2 \phi_{DK}, \tag{5.14d}
\end{aligned}$$

with $J_{\parallel} = N_{DK} (U_{\parallel iDK1} - U_{\parallel eDK1})$. Finally, through tedious elementary vector calculus and algebra, we get

$$\begin{aligned}
\partial_t \Omega &= \nabla_{\parallel} J_{\parallel} - \nabla_{\parallel} (\Omega U_{\parallel iDK}) - \frac{1}{B} [\phi_{DK} + \phi_{GK}, \Omega] - \frac{1}{2m_i \Omega_i^2} \nabla_{\parallel} (P_{\perp iDK} \nabla_{\perp}^2 U_{\parallel iDK}) \\
&\quad - \frac{1}{B} [\nabla_{\perp} (\phi_{DK} + \phi_{GK}) \cdot, \boldsymbol{\omega}] - \nabla_{\parallel} (\boldsymbol{\omega} \cdot \nabla_{\perp} U_{\parallel iDK}) + \frac{1}{B \Omega_i} \nabla_{\perp} S_N \cdot \nabla_{\perp} \phi_{DK} \\
&\quad + \frac{1}{B^2 \Omega_i} [\nabla_{\perp} \phi_{DK} \cdot, N_{iDK} \nabla_{\perp} \phi_{GK}] + \frac{1}{2m_i \Omega_i^2} [\nabla_{\perp}^2 \phi_{GK}, P_{\perp iDK}] \\
&\quad - \frac{1}{2m_i \Omega_i^2} \nabla_{\parallel} (\nabla_{\perp}^2 Q_{\perp iDK}), \tag{5.14e}
\end{aligned}$$

with

$$\boldsymbol{\omega} = \frac{1}{B \Omega_i} N_{DK} \nabla_{\perp} \phi_{DK} + \frac{1}{m_i \Omega_i^2} \nabla_{\perp} P_{\perp iDK}, \tag{5.14f}$$

and as a consequence

$$\Omega = \nabla_{\perp} \cdot \boldsymbol{\omega}. \tag{5.14g}$$

Since Eq. (5.14e) requires J_{\parallel} to first non-vanishing order, we derive an equation for J_{\parallel} , describing it as a dynamical field. Noticing that

$$\begin{aligned}
J_{\parallel} &\equiv N_{DK} (U_{\parallel iDK} - U_{\parallel eDK}) \\
&= N_{DK} (U_{\parallel iDK1} - U_{\parallel eDK1}) \sim \mathcal{O}(N_{DK} c_s \epsilon_{\perp}^2, N_{DK} c_s \epsilon_m^2), \tag{5.15a}
\end{aligned}$$

we remark that that J_{\parallel} is the DK current density and does not include the GK distribution functions. Taking the derivative of Eq. (5.15a), we get

$$\begin{aligned} \partial_t J_{\parallel} + \frac{1}{B} [\phi_{DK} + \phi_{GK}, J_{\parallel}] + \nabla_{\parallel} (J_{\parallel} U_{\parallel}) + J_{\parallel} \nabla_{\parallel} U_{\parallel} + \frac{e}{m_e} N_{DK} \nabla_{\parallel} \phi_{DK} + \frac{1}{m_i} \nabla_{\parallel} P_{\parallel iDK} \\ + \frac{1}{m_e} \nabla_{\parallel} (N_{DK} T_{eDK}) = \frac{S_N}{N_{DK}} J_{\parallel} - \nu_{\parallel} \frac{N_{DK} m_i}{N_0 m_e} J_{\parallel} - 0.71 \frac{N_{DK}}{m_e} \nabla_{\parallel} T_{eDK} + S_J, \end{aligned} \quad (5.15b)$$

having introduced the source term, $S_j \equiv \int d\mathbf{v} ((v_{\parallel} - U_{\parallel iDK}) S_i - (v_{\parallel} - U_{\parallel eDK}) S_e)$ and the Spitzer resistivity $\nu_{\parallel} = \nu_0 (T_e/T_{e0})^{-3/2}$.

Eqs. (5.14e) and (5.15b) are equivalent to the vorticity and current density equation for the drift-reduced Braginskii model Zeiler *et al.* (1997) except for the addition of the source term, $\sim \nabla_{\perp} S_N$, arising from considering the presence of sources, and the terms $\sim \nabla_{\parallel} (P_{\perp iDK} \nabla_{\perp}^2 U_{\parallel iDK} + \nabla_{\perp}^2 Q_{\perp iDK})$ in Eq. (5.14e) due to the distinction between particle and gyrocenter parallel velocity. In this work, we use the gyrocenter parallel velocity while in drift-reduced Braginskii equations, the particle parallel velocity is used. We remark that the term $T_{eDK} \nabla_{\parallel} J_{\parallel} / N_{eDK} \sim \epsilon_{\perp}^2 \partial_t T_e$ in Eq. (3.5b) is of higher order, therefore we choose to neglect it in our simulations.

Finally, in order to obtain an equation for ϕ_{GK} , we evaluate the order ϵ_{δ} terms in Eq. (5.2a) and insert N_{eGK} from Eq. (4.2)

$$\varrho_i^* = \frac{e\phi_{GK}}{T_{eDK}} N_{DK} - \frac{q_i}{B} \left\| \partial_{\mu} \langle \langle \phi_{GK} \rangle_{\mathbf{R}} \rangle_{\mathbf{x}}^{\dagger} \right\|. \quad (5.16)$$

We note that the left hand side of Eq. (5.16) only depends on \mathcal{N}_{iGK}^{pj} while the right hand side is an operator, depending on the DK fields, acting on ϕ_{GK} . In the limit where the DK distribution functions are constant Maxwellians, Eq. (5.16) reduces to the standard δ -f GK Poisson equation

$$\varrho_i^* = eN_{DK} \left[\frac{1}{T_{eDK}} + \frac{1}{T_{iDK}} - \frac{1}{T_{iDK}} \exp\left(-\frac{T_{iDK} k_{\perp}^2}{m_i \Omega_i^2}\right) I_0\left(\frac{T_{iDK} k_{\perp}^2}{m_i \Omega_i^2}\right) \right] \phi_{GK}, \quad (5.17)$$

with I_0 the modified Bessel function of order zero.

6. Simulation setup and numerical implementation

In order to implement the system of Eqs. (3.5a), (3.5b), (3.10a) for $(p, j) \neq (0, 0)$ and $(p, j) \neq (1, 0)$, (4.4a), (5.8b), (5.14e), (5.14g), (5.15b), and (5.16), closed by enforcing $\mathcal{N}_{iDK}^{00} = N_{eDK} = N_{DK}$, $\mathcal{N}_{iDK}^{10} = 0$, and $U_{\parallel iDK} = U_{\parallel eDK} = U_{\parallel}$, we normalize time, t , to R/c_{s0} ($c_{s0} = \sqrt{T_{e0}/m_i}$ is the ion sound speed at the constant reference electron temperature, T_{e0} , and R is the characteristic length that indicates the size of the plasma

chamber in the direction perpendicular to \mathbf{B}). The electrostatic potentials, ϕ_{DK} and ϕ_{GK} , are normalized to T_{e0}/e , the parallel (to \mathbf{B}) spatial scale to R , and the perpendicular ones to $\rho_{s0} = c_{s0}/\Omega_i$. The densities, N_{DK} and N_{GK} , are normalized to the constant reference density N_0 , the parallel fluid velocities, U_{\parallel} , to c_{s0} , the electron and ion temperatures, T_e , $T_{\parallel i}$, and $T_{\perp i}$, to T_{e0} , T_{i0} , and T_{i0} , respectively. Finally, we normalize the parallel current density, J_{\parallel} , to $N_0 c_{s0}$.

The domain we consider is a cuboid with sides L_x , L_y , and L_z . We introduce the spatial coordinates (x, y, z) , where z is parallel to the magnetic field of the device, and x and y are perpendicular to z , forming a right-handed coordinate system.

To evolve the DK quantities, \mathcal{N}_{iDK}^{pj} , U_{\parallel} , N_{DK} , T_{eDK} , ϕ_{DK} , Ω and J_{\parallel} , we use a finite-difference scheme similar to the one described in Ref. Frei *et al.* (2024); Mencke & Ricci (2025). The x direction is discretized in N_x equally sized grid points such that the grid spacing is $\Delta x = L_x/N_x$. An equivalent discretization is used for y and z . Similarly to the GBS code Giacomini *et al.* (2022), derivatives are calculated with a fourth order central difference scheme, except for the Poisson bracket operator, $[f, g]$, which is evaluated using the fourth-order Arakawa algorithm Arakawa (1997). A staggered grid approach Paruta *et al.* (2018) is used in the z direction with U_{\parallel} , J_{\parallel} , and the \mathcal{N}_{iDK}^{pj} with odd p being evolved on grid points shifted by a distance $\Delta z/2$ with respect to the grid points for N_{DK} , T_{eDK} , ϕ_{DK} , Ω , and \mathcal{N}_{iDK}^{pj} with even p .

To evolve the GK fields, \mathcal{N}_{iGK}^{pj} and ϕ_{GK} , we use a spectral method in the (x, y) plane, and finite differences along z . More precisely, we evolve $N_{kx} \times \lfloor N_{ky}/2 + 1 \rfloor$ Fourier modes with wavevectors k_x and k_y with spacing $\Delta k_x = 2\pi/L_x$ and $\Delta k_y = 2\pi/L_y$, respectively. Non-linear terms are evaluated in real space by inverse Fourier transforming the fields, multiplying them, and Fourier transforming back. All Fourier transforms are performed with the FFTW library Frigo & Johnson (2005). We note that ϕ_{GK} and \mathcal{N}_{iGK}^{pj} with even p are evolved on the same z -coordinates as ϕ_{DK} , while the \mathcal{N}_{iGK}^{pj} with odd p are evolved on the same z -coordinates as U_{\parallel} . Finally, all fields are antialiased using the 2/3 rule Hoffmann *et al.* (2023b,a); Orszag (1971).

For the DK and GK gyromoments, we close the hierarchy using a simple truncation approach. Thus, we evolve \mathcal{N}_{iDK}^{pj} with p from 0 to P_{DK} and with j from 0 to J_{DK} for the DK moments. Similarly, for the GK moments, we evolve \mathcal{N}_{iGK}^{pj} with p from 0 to P_{GK} and with j from 0 to J_{GK} .

Similarly to Mencke & Ricci (2025), a fifth-order adaptive time-step Runge-Kutta

scheme is used to advance all fields Press *et al.* (1992). Equation (5.14g) is solved for ϕ_{DK} using an approach similar to the one used in the two-fluid GBS code Giacomini *et al.* (2022). The discrete operator of the $\nabla \cdot (N_{DK} \nabla \phi_{DK})$ term is constructed at each time step and the linear system is solved for ϕ_{DK} using the PETSCs library Balay *et al.* (2024). Equation (5.16) is solved for ϕ_{GK} using an iterative approach. Since the electron adiabatic response generally dominates the right hand side of Eq. (5.16), for each z plane we solve

$$\phi_{GK}^{n+1} = \frac{T_{eDK}}{N_{eDK}} \left(\rho_i^* + \frac{q_i}{B} \left\| \partial_\mu \langle \langle \phi_{GK}^n \rangle_{\mathbf{R}} \rangle_{\mathbf{x}}^\dagger \right\|_i \right)$$

while: $\max_{k_x, k_y} |\phi_{GK}^{n+1} - \phi_{GK}^n| > \eta_{GK}$, (6.1)

and initialize ϕ_{GK}^0 using ϕ_{GK} from the previous timestep. The parameter $\eta_{GK} > 0$ is the error threshold chosen small enough not to impact the results (typically $\eta_{GK} \sim 10^{-7}$).

For stability reasons, numerical diffusion is added to the right-hand side of all equations for all evolved DK fields, f , that is

$$D(f) = \eta_\perp (\partial_x^2 + \partial_y^2) f + \eta_z \partial_z^2 f. \quad (6.2)$$

The numerical parameter $\eta_\perp > 0$ and $\eta_z > 0$ are chosen as small as possible to guarantee the numerical stability of the simulations, without significantly affecting the results. For the GK field, we do not add numerical diffusion in the perpendicular plane, i.e. $\eta_\perp = 0$. However, we do include numerical diffusion in the z -direction.

Following the approach of Frei *et al.* (2024) and Mencke & Ricci (2025), we use Bohm fluid boundary conditions for U_\parallel and J_\parallel Loizu *et al.* (2012); Masetto *et al.* (2015) at the sheath entrances

$$U_\parallel(z = \pm L_z/2) = \pm c_s$$

$$= \pm \sqrt{T_{eDK} + \tau_i T_{iDK}}, \quad (6.3a)$$

$$J_\parallel(z = \pm L_z/2) = \pm N_{DK} \left(c_s - \sqrt{T_{eDK}} e^{\Lambda - \phi_{DK}/T_{eDK}} \right), \quad (6.3b)$$

while homogeneous Neumann boundary conditions are used for the remaining boundaries for J_\parallel and U_\parallel . For all other DK fields, homogeneous Neumann boundary conditions are applied at all boundaries while we apply homogeneous Neumann boundary conditions in the parallel direction for the GK fields and periodic boundary conditions in the perpendicular plane.

The plasma sources are chosen as

$$S_i = A_N(\mathbf{x}) F_{Mi} + A_E(\mathbf{x}) \left(s_{\parallel i}^2 + x_i - \frac{3}{2} \right) N_{DK} F_{Mi}, \quad (6.4a)$$

where $\langle\langle A_N(\mathbf{x}) \rangle\rangle_{\mathbf{R}} = A_N$ is assumed and analogously for A_E . Therefore, we order S_i on the DK timescale ($S_i \sim \partial_t F_{iDK}$). The projection in the DK hierarchy, Eq. (3.12a), is

$$S_{i0}^{pj} = A_N(\mathbf{R}) \delta_{00}^{pj} + \frac{\delta_{20}^{pj}}{\sqrt{2}} N_{DK} A_E(\mathbf{R}) - \delta_{01}^{pj} N_{DK} A_E(\mathbf{R}), \quad (6.4b)$$

and the projections in the GK hierarchy, Eq. (4.4a), is given by

$$\begin{aligned} \delta S_{i1}^{pj} = & \delta_0^p \left(K_j(b_i) - \delta_0^j \right) A_N + \frac{\delta_2^p}{\sqrt{2}} N_{DK} \left(K_j(b_i) - \delta_0^j \right) A_E \\ & + \delta_0^p N_{DK} \left(2j K_j(b_i) - (j+1) K_{j+1}(b_i) - j K_{j-1}(b_i) + \delta_1^j \right) A_E. \end{aligned} \quad (6.4c)$$

For the electrons in Eqs. (3.5a) and (3.5b), the sources are

$$S_N = A_N(\mathbf{R}), \quad S_{Te} = A_{Te}(\mathbf{R}), \quad (6.4d)$$

with

$$K_n(x) = \frac{1}{n!} \left(\frac{x}{2} \right)^{2n} e^{-(x/2)^2}, \quad \text{and} \quad b_i = \frac{v_{Thi} k_{\perp}}{\Omega_i}. \quad (6.4e)$$

Finally, we do not include a momentum source such that $S_U = 0$ in Eq. (5.8b).

Simulations that solve the full system, including DK and GK fluctuations, are referred to as full simulations. For comparison, simulations are run where $\mathcal{N}_{iGK}^{pj} = 0$ and $\phi_{GK} = 0$. These are referred to as DK simulations.

We start the simulations from smooth analytical profiles satisfying the boundary conditions in Eq. (6.3) and evolve the DK simulations at first. Quasi-steady state is achieved after approximately $165 c_{s0}/R$ time units using a small number of gyromoments ($P_{DK} = 2$ and $J_{DK} = 1$). Afterwards, the number of moments, P_{DK} and J_{DK} , is increased and the evolution of ϕ_{GK} and \mathcal{N}_{iGK}^{pj} is included. We choose $P_{DK} = 2J_{DK}$ for the DK moments and $P_{GK} \lesssim J_{GK}$ for the GK moments to study the influence of FLR effects on the simulations. When a quasi-steady state is reached, the particles and energy injected by the sources are transported slowly across the field lines by turbulent transport and rapidly along the field lines to the sheaths where the plasma outflow at the sheath entrances balances the sources. All analyses are carried out during this quasi-steady state.

For our simulations, we consider a helium LAPD plasma Gekelman *et al.* (1991) with parameters as in Refs. Rogers & Ricci (2010); Frei *et al.* (2024); Mencke & Ricci (2025). The simulation parameters are: $n_{e0} = 2 \times 10^{12} \text{ cm}^{-3}$, $T_{e0} = 6 \text{ eV}$, $T_{i0} = 3 \text{ eV}$, $\Omega_i \sim 960 \text{ kHz}$, $\rho_{s0} = 1.4 \text{ cm}$, $c_{s0} = 1.3 \times 10^6 \text{ cm/s}$, $m_i/m_e = 400$, $\nu_0 = 0.03$, and $\tau_i = 0.5$. The

LAPD vacuum chamber has a radius $R \simeq 0.56$ m, therefore we assume $R = 40\rho_{s0}$ and, with a parallel extension $L_z \simeq 18$ m, we impose $L_z = 36R$. With these parameters, the reference time is $R/c_{s0} \sim 43 \mu\text{s}$. We set the perpendicular extension of the domain $L_x = L_y = 100\rho_{s0}$, sufficiently large for the turbulent structures not to be affected by the perpendicular boundary conditions. We choose our sources in Eq. (6.4) to have radial extension from the axis r_s and radial gradient length L_s , that is

$$A_N(x, y) = \frac{\mathcal{A}_{N0}}{2} \left[1 - \tanh\left(\frac{r - r_s}{L_s}\right) \right] + \mathcal{A}_{N\infty}, \quad (6.5)$$

where $r = \sqrt{x^2 + y^2}$ and equivalent expressions are used for A_E , A_{T_e} , and \mathcal{A}_N with \mathcal{A}_{N0} , \mathcal{A}_{E0} , and \mathcal{A}_{T_e0} representing the bulk plasma sources. The constant terms, $\mathcal{A}_{N\infty}$, $\mathcal{A}_{E\infty}$, $\mathcal{A}_{T_e\infty} \ll \mathcal{A}_{N0}$, $\mathcal{A}_{T_{i0}}$, \mathcal{A}_{T_e0} , avoid negative values of temperature and density and are chosen to have small amplitude. The source parameters are chosen as $\mathcal{A}_{N\infty} = \mathcal{A}_{T_e\infty} = 0.004$, $\mathcal{A}_{E\infty} = 0.001$, $\mathcal{A}_{N0} = \mathcal{A}_{T_e0} = \mathcal{A}_{E0} = 0.04$, $L_s = 1\rho_{s0}$, $r_s = 20\rho_{s0}$.

The perpendicular grid resolution is $N_x = N_y = 192$, which corresponds to a grid spacing of $\sim 0.52\rho_{s0}$. The number of parallel grid points is $N_z = 64$, which corresponds to a grid spacing of $\sim 0.56R$. For the DK fields (n_e , T_e , U_{\parallel} , Ω , J_{\parallel} , and \mathcal{N}_{iDK}^{pj}) diffusion parameters are chosen as $\eta_{zDK} \simeq 4$ and $\eta_{\perp} \simeq 0.5$. For the Fourier grid, we impose $N_{k_x} = N_{k_y} = 96$ such that $\max(k_x) = \max(k_y) = 3.08/\rho_{s0}$. For \mathcal{N}_{iGK}^{pj} , $\eta_{zGK} \simeq 4$ is the same value as for the DK fields. We note that no numerical diffusion for the GK fields is required since the $\nabla_{\perp}^2 \mathcal{N}_{iGK}^{pj}$ term in Eq. (4.5) provides sufficiently large damping for high k_{\perp} modes and also ensures strong damping for modes with $k_{\perp} \gtrsim 1/\rho_{s0}$. Finally, we use $\eta_{GK} = 10^{-7}$.

7. Simulation results

In this section, we present simulations based on the model described in Secs. 3, 4, and 5, using the parameters of the LAPD experiment described in Sec. 6. We show the equilibrium DK and GK gyromoments in Sec. 7.1. In Sec. 7.2 we demonstrate spectral convergence of our simulations by comparing the ion distribution function with a local bi-Maxwellian and by investigating the effect of the number of gyromoments on the statistical properties of ϕ_{DK} . We investigate the turbulence properties of the DK fields in Sec. 7.3. Finally, in Sec. 7.4 we analyze the properties of the GK fields.

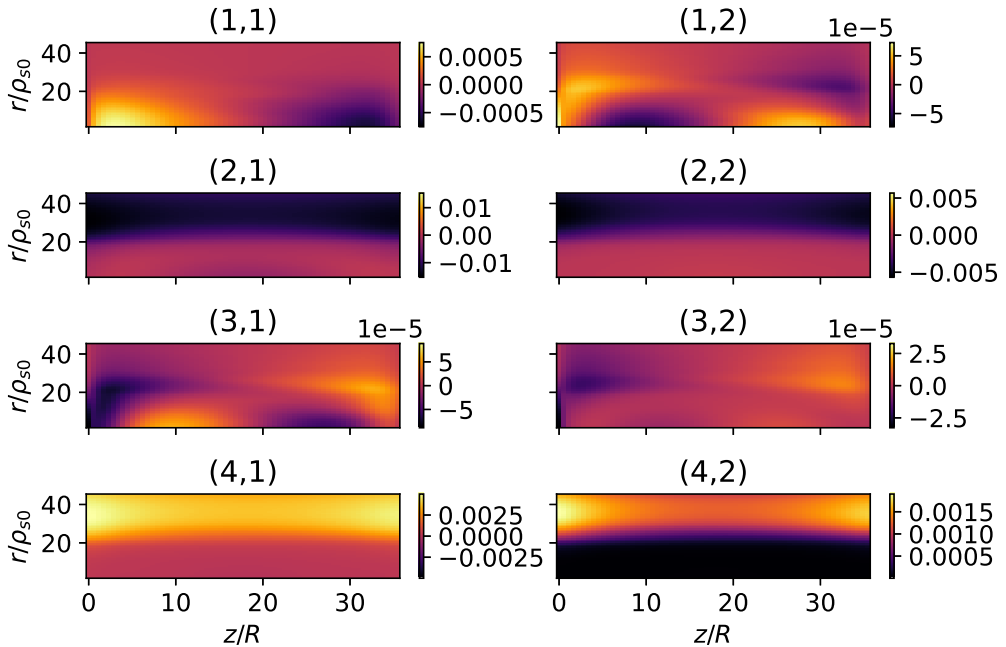


FIGURE 1. The spatial and azimuthal average of the DK moments, $\langle \mathcal{N}_{iDK}^{pj} \rangle_{t,\vartheta}$, for a full simulation with $(P_{DK}, J_{DK}, P_{GK}, J_{GK}) = (6, 3, 6, 5)$ for $p = 1-4$ (rows) and $j = 1, 2$ (columns). Moments with odd p are antisymmetric around $z = L_z/2$ and moments with even p are symmetric around $z = L_z/2$.

7.1. Equilibrium gyromoments

The spatial and azimuthal average, defined as

$$\langle \cdot \rangle_{t,\vartheta} = \frac{1}{2\pi} \int_0^{2\pi} d\vartheta \frac{1}{\Delta t} \int_{t_0}^{t_0+\Delta t} dt (\cdot), \quad (7.1)$$

of the DK gyromoments, $\langle \mathcal{N}_{iDK}^{pj} \rangle_{t,\vartheta}$, with $\vartheta = \arctan y/x$ are shown in Fig. 1. The gyromoments with odd (even) p are antisymmetric (symmetric) around $z = L_z/2$. Furthermore, the amplitude of the moments decreases with p and j . We note that the plasma equilibrium is very similar to previous gyromoment simulations of an LAPD plasma Mencke & Ricci (2025).

Figure 2 shows the spatial and azimuthal average of the GK moments, $\langle \mathcal{N}_{iGK}^{pj} \rangle_{t,\vartheta}$. Similar symmetry properties as for the DK moments are observed, although the GK moments have significantly smaller amplitude. Furthermore, the amplitude of $\langle \mathcal{N}_{iGK}^{pj} \rangle_{t,\vartheta}$ is localized around the source gradient $r \sim 20\rho_{s0}$ since δS_{i1}^{pj} is the largest in that region.

In order to quantify the kinetic part of the distribution function, we compare the moments from the full simulations with those of a local bi-Maxwellian Mencke & Ricci

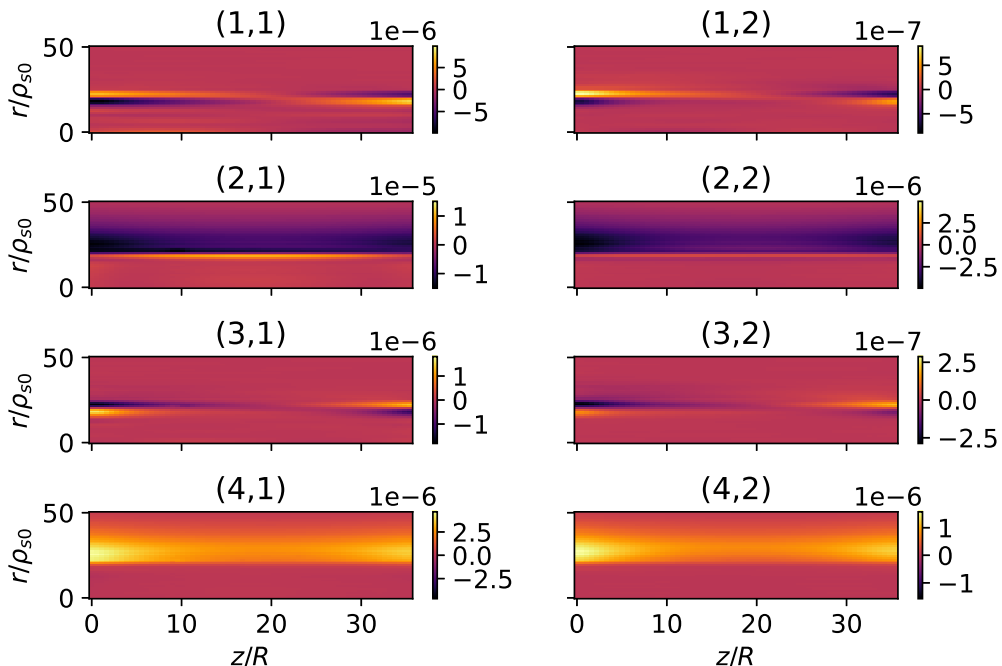


FIGURE 2. The spatial and azimuthal average of \mathcal{N}_{iGK}^{pj} , $\langle \mathcal{N}_{iGK}^{pj} \rangle_{t,\vartheta}$, for a full simulation with $(P_{DK}, J_{DK}, P_{GK}, J_{GK}) = (6, 3, 6, 5)$ for $p = 1 - 4$ (rows) and $j = 1, 2$ (columns). Moments with odd p are antisymmetric around $z = L_z/2$ and moments with even p are symmetric around $z = L_z/2$.

(2025)

$$F_{bM} = \frac{N_i m_i^{3/2}}{(2\pi)^{3/2} \sqrt{T_{\parallel} T_{\perp i}}} \exp \left(-\frac{m_i (v_{\parallel} - U_{\parallel i})^2}{T_{\parallel i}} - \frac{\mu B}{T_{\perp i}} \right), \quad (7.2a)$$

with the projection on the Hermite-Laguerre basis in Eq. (3.6a) given by

$$\mathcal{N}_{bM}^{pj} = \begin{cases} N_i \frac{(-1)^j \sqrt{p!}}{\sqrt{2^p (p/2)!}} \left(\frac{T_{\parallel i}}{T_{i0}} - 1 \right)^{p/2} \left(\frac{T_{\perp i}}{T_{i0}} - 1 \right)^j & \text{for even } p, \\ 0 & \text{for odd } p. \end{cases} \quad (7.2b)$$

We use the local $T_{\perp i}$, $T_{\parallel i}$, and $N_i = N_{DK}$ in Eq. (7.2b) and show the spatially maximal deviation for the gyromoments in the full-f simulation for each p and j in Fig. 3. Small deviations are observed due to the high collisionality in the simulations, similarly to DK-ordered gyromoment simulations of the same system Mencke & Ricci (2025).

7.2. Convergence study

Since deviations from a bi-Maxwellian are small, a small number of moments is needed to reach convergence. We investigate the statistical properties of the DK electrostatic

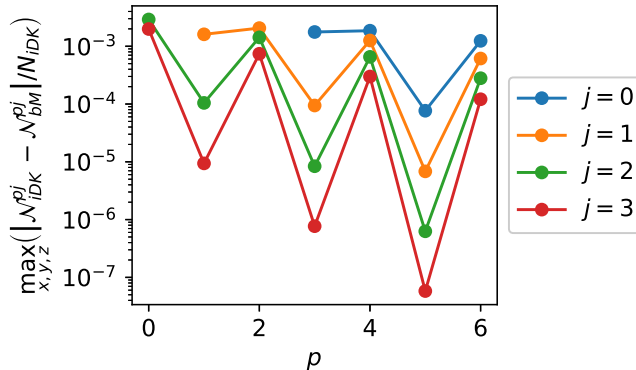


FIGURE 3. The spatial maximum of the difference between the DK moments and the moments of a bi-Maxwellian calculated using Eq. (7.2b) with the local parallel and perpendicular temperatures normalized to the local density for $(P_{DK}, J_{DK}, P_{GK}, J_{GK}) = (6, 3, 6, 5)$. Small deviations from a bi-Maxwellian are observed.

potential, ϕ_{DK} , and how these are affected by the number of evolved moments in Fig. 4. We compare the temporal and azimuthal average of ϕ_{DK} , defined in Eq. (7.1), the root mean square,

$$RMS(\phi_{DK}) = \sqrt{\left\langle \left((\phi_{DK}) - \langle \phi_{DK} \rangle_{t,\vartheta} \right)^2 \right\rangle_{t,\vartheta}}, \quad (7.3a)$$

and the skewness

$$SKW(\phi_{DK}) = \left\langle \left((\phi_{DK}) - \langle \phi_{DK} \rangle_{t,\vartheta} \right)^3 \right\rangle_{t,\vartheta} / RMS^3(\phi_{DK}), \quad (7.3b)$$

for different choices of $P_{DK}, J_{DK}, P_{GK}, J_{GK}$ and for the full and DK simulations. It is observed that spectral convergence is obtained at $(P_{DK}, J_{DK}) = (2, 1)$ for both the full and DK simulations and the average, RMS, and skewness of ϕ_{DK} are not significantly affected by the presence of GK fields. A similar trend is observed for all other DK fields. Both models and all choices of (P_{DK}, J_{DK}) display a negative skewness at $r \lesssim 20\rho_{s0}$, associated with the propagation of holes, and a positive skewness for $r \gtrsim 20\rho_{s0}$, associated with blobs, similar to simulations of the tokamak boundary. Similar statistical behavior of the fields was reported in previous simulations of LAPD plasmas Frei *et al.* (2024); Mencke & Ricci (2025). In the following, we analyse the results of the simulations with $(P_{DK}, J_{DK}) = (6, 3)$.

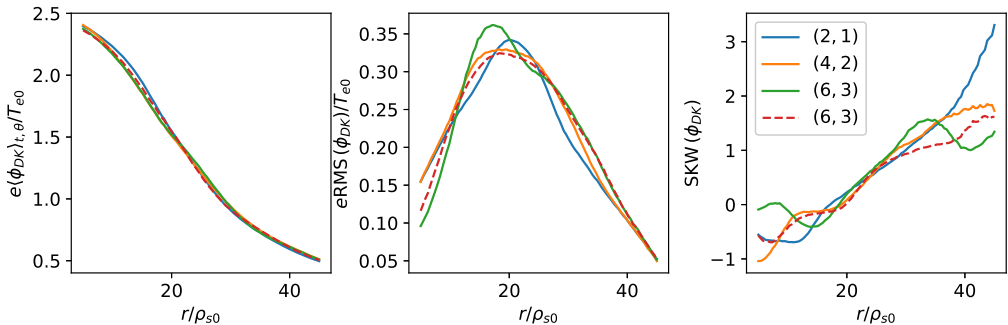


FIGURE 4. The azimuthal and temporal average, root mean square, and skewness of ϕ_{DK} at $z = L_z/2$ for different choices of $(P_{DK}, J_{DK}, P_{GK}, J_{GK})$. For the GK simulations, $P_{DK} = P_{GK}$ and $J_{GK} = 5$. The full (solid) and DK (dashed) models are compared. The simulations are considered converged at $(P_{DK}, J_{DK}) = (2, 1)$. The presence of GK fields does not impact ϕ_{DK} noticeably.

7.3. Properties of the DK fields

We consider the turbulent behavior of the DK fields. Figure 5 shows a perpendicular snapshot of the DK fields for the full simulation, while Fig. 6 shows the same snapshot for the DK simulation. We note that for both simulations, all fields display large turbulent structures in the perpendicular plane. The DK and full simulations are very similar, indicating that the inclusion of the GK fields do not significantly affect the system. A snapshot of the DK fields in the parallel plane is shown in Fig. 7 for the full simulations. We observe elongated structures in the z -direction. Similar properties are observed for the DK simulations (not shown here).

Figure 8 compares the power spectrum of Ω as a function of the parallel wave number, k_z , and azimuthal mode number, m . We observe low- m modes elongated in z . The full and DK simulations have similar power spectrum. To test the interaction between DK and GK fields, we artificially lower the collisionality in Eq. (4.5) by a factor of 1000, setting $\nu_{i0} \sim 0.00234c_{s0}/R$, and we increase A_E and A_N by a factor 10 in Eq. (6.4c). By reducing the GK collisional term and increasing the GK source term, we observe an increase in high m modes indicating that in a system with lower collisionality and larger sources, the GK fields can introduce high k_\perp -modes in the DK fields.

7.4. Properties of gyrokinetic fields

In Fig. 9, ϕ_{GK} is shown in real space (x, y, z) while Fig. 10 shows ϕ_{GK} in (k_x, k_y, z) space. The GK potential, ϕ_{GK} , depends weakly on the z -direction and is dominated by

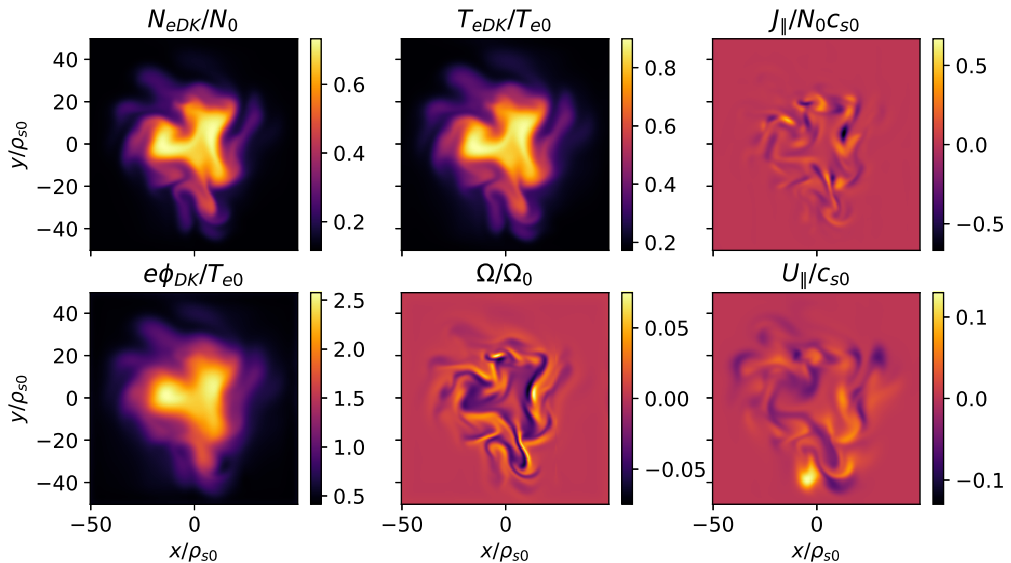


FIGURE 5. Perpendicular, (x, y) , snapshot of N_{DK} (top left), T_{eDK} (top center), J_{\parallel} (top right), ϕ_{DK} (bottom left), Ω (bottom center), and U_{\parallel} (bottom right) for a full simulation with $(P_{DK}, J_{DK}, P_{GK}, J_{GK}) = (6, 3, 6, 5)$ at $z = L_z/2$. Turbulent structures are observed at the source-gradient region ($r \sim r_s \sim 20\rho_{s0}$).

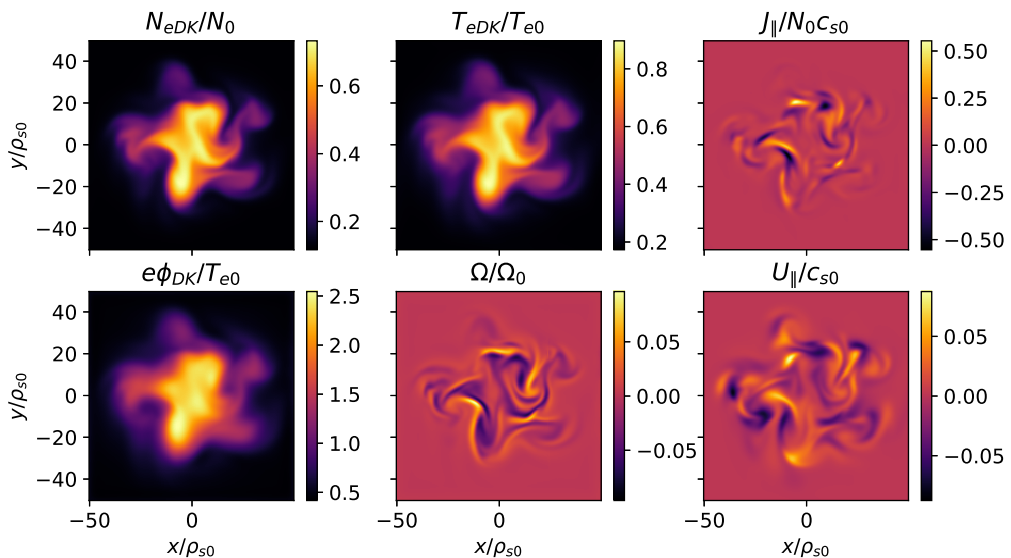


FIGURE 6. Same as Fig. 5 for a DK simulation with $(P_{DK}, J_{DK}) = (6, 3)$. Similar structures as for the full model in Fig. 5 are observed.

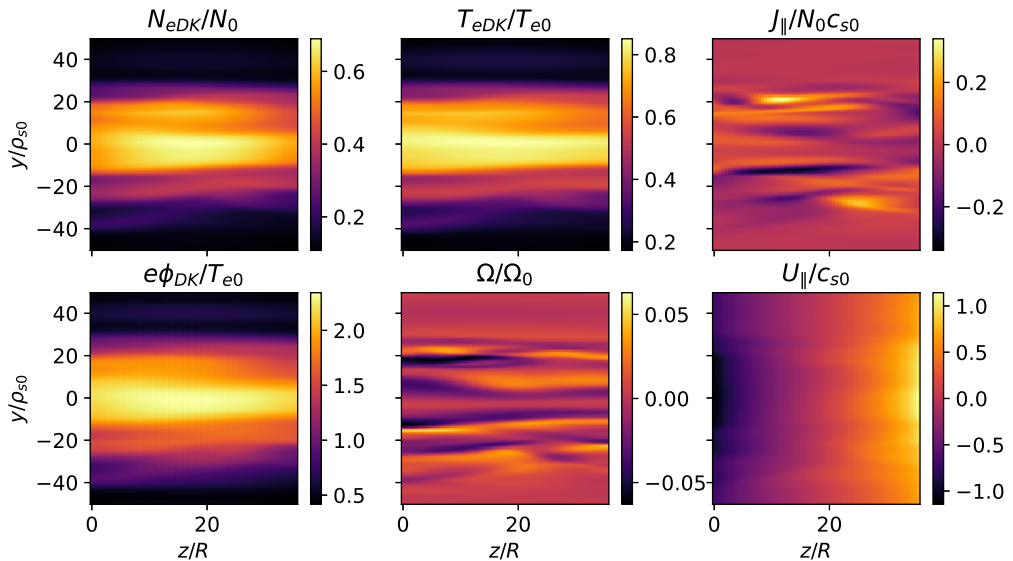


FIGURE 7. Parallel, (z, y) , snapshot of N_{DK} (top left), T_{eDK} (top center), $J_{||}$ (top right), ϕ_{DK} (bottom left), Ω (bottom center), and $U_{||}$ (bottom right) for a full simulation with $(P_{DK}, J_{DK}, P_{GK}, J_{GK}) = (6, 3, 6, 5)$ at $x = 0$. The turbulent structures are very elongated along z .

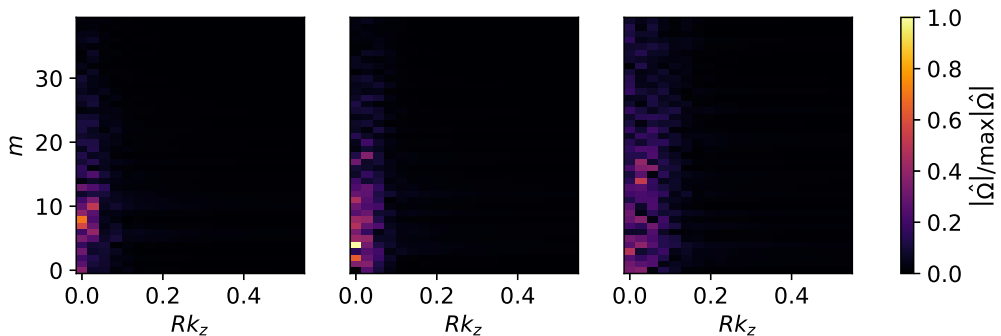


FIGURE 8. Power spectrum of $\Omega = \sum_{m,\omega} \hat{\Omega} e^{i(m\vartheta + k_z z)}$ at the radial distance, $r = \sqrt{x^2 + y^2} = 20\rho_{s0}$ for a full simulation with $(P_{DK}, J_{DK}, P_{GK}, J_{GK}) = (6, 3, 6, 5)$ (left), the DK simulation with $(P_{DK}, J_{DK}) = (6, 3)$ (center), and a full simulation with ν_{i0} in Eq. (4.5) reduced by a factor of 1000 and with A_E and A_N increased by a factor 10 in Eq. (6.4c) (right).

$k_{\perp}\rho_s \lesssim 1$ modes. Comparing with Fig. 5, it is seen that ϕ_{GK} is one order of magnitude smaller than ϕ_{DK} and from Fig. 10, $k_{\perp}\rho_{s0} \sim 1$ modes are observed to exist even though they are not dominant. This is consistent with the ordering imposed in Sec. 2. Due to the high collisionality, the spatial diffusion induced by the $\nabla_{\perp}^2 \mathcal{N}_{iGK}^{pj}$ term in Eq. (4.5)

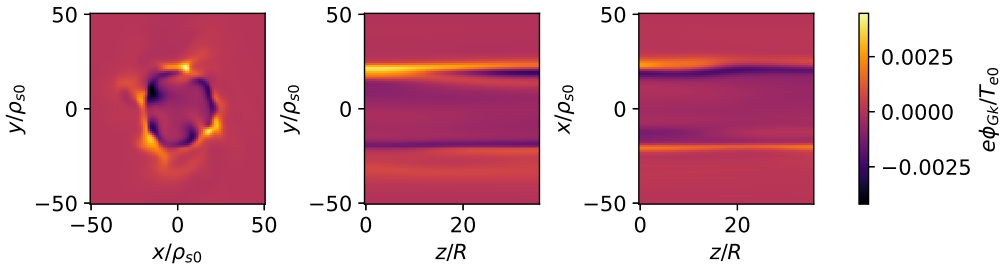


FIGURE 9. Snapshots of ϕ_{GK} in real space at $z = L_z/2$ (left), $x = 0$ (middle), and $y = 0$ (right) for $(P_{DK}, J_{DK}, P_{GK}, J_{GK}) = (6, 3, 6, 5)$. We note that ϕ_{GK} has small amplitude with small scale structures in the perpendicular plane and is almost constant along z .

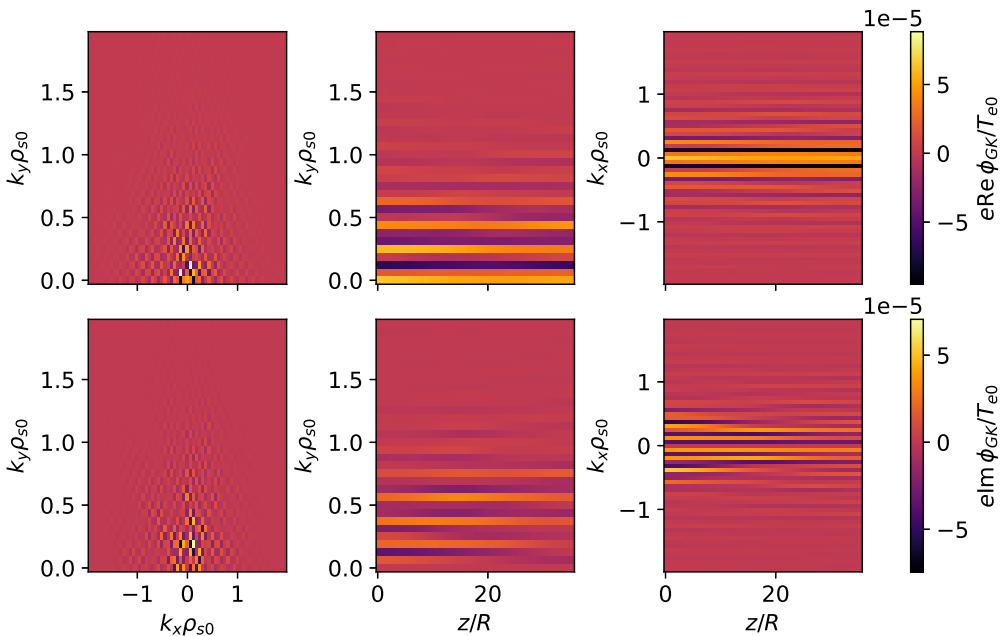


FIGURE 10. Snapshots of ϕ_{GK} in Fourier (k_x, k_y, z) space at $z = 0$ (left), $k_x = 0$ (middle), and $k_y = 0$ (right) real part (top) and imaginary part (bottom) for $(P_{DK}, J_{DK}, P_{GK}, J_{GK}) = (6, 3, 6, 5)$.

suppresses high k_{\perp} modes for \mathcal{N}_{iGK}^{pj} . Since in Eq. (5.16), $\rho_i^* \propto \exp(-2T_{i0}k_{\perp}^2/m_i\Omega_i^2)$ [see Eq. (B1b)], we further dampen high k_{\perp} modes in ϕ_{GK} .

Finally, the amplitude of the GK moments are shown in Fig. 11. The amplitude of the moments, \mathcal{N}_{GK}^{pj} , rapidly decreases with p and j . This is due to the large collisionality which suppresses high p and j moments, as seen from Eq. (4.5).

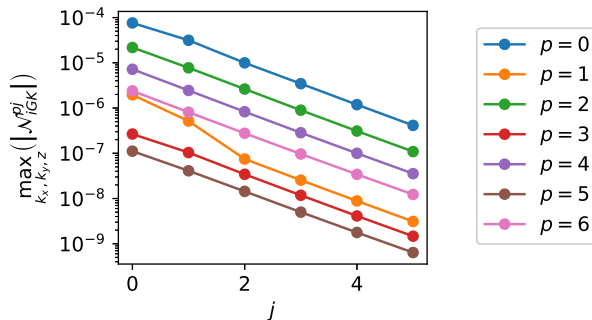


FIGURE 11. Spatial maximum of the amplitude of the GK moments, $\max_{k_x, k_y, z} (|\mathcal{N}_{iGK}^{pj}|)$, for $(P_{DK}, J_{DK}, P_{GK}, J_{GK}) = (6, 3, 6, 5)$. The magnitude quickly decreases with p and j .

8. Linear analysis of the turbulent modes

For studying the turbulent behavior of the simulations observed in Fig. 8, the system of Eqs. (3.5a), (3.5b), (3.10a), (4.4a), (5.8b), (5.14e), (5.14g), (5.15b), and (5.16) is linearized. Specifically, each DK field, f_{DK} , is split as

$$f_{DK} = \bar{f}_{DK}(r) + \tilde{f}_{DK}(r) e^{i(m\vartheta + k_{\parallel}z - \omega t)}, \quad (8.1)$$

where the equilibrium, \bar{f}_{DK} , is calculated from the full 3D turbulent simulations by performing a temporal and azimuthal averaging at $z = L_z/2$. For the GK field, f_{GK} , we apply a local approximation,

$$f_{GK} = \bar{f}_{GK}(r) + \tilde{f}_{GK} \delta(r - r_g) e^{i(m\vartheta + k_{\parallel}z - \omega t)}, \quad (8.2)$$

where r_g is the radial position at which the GK fluctuations are localized. To calculate \bar{f}_{GK} we first perform an inverse Fourier transform in the perpendicular plane of the fields in the global full 3D simulations. Then, the temporal and azimuthal averaging at $z = L_z/2$ are evaluated.

In Fig. 12 we show the dominant linear growth-rate, $\gamma \equiv \text{Im} \omega$, as function of k_{\parallel} and m for the full model, the DK model (where we impose $\mathcal{N}_{iGK}^{pj} = 0$ and $\phi_{GK} = 0$), and the GK model (where we impose $\tilde{f}_{DK} = 0$). We only consider $m \leq 40$ since the numerical diffusion for the DK field significantly dampens modes with higher m . The equilibrium fields, \bar{f} , for the DK model are calculated using the simulations with physical collisionality and sources. With the physical parameters, the full model yields linear growth rates identical to that of the DK model while the GK model is stable for all choices of m and k_{\parallel} . For this reason, for the full and GK model, we calculate the equilibrium fields using the

simulations where ν_{i0} in Eq. (4.5) is reduced by a factor of 1000 and where A_E and A_N are increased by a factor 10 in Eq. (6.4c). Furthermore, we neglect \mathcal{C}_{ii}^{pj} in Eq. (4.4a).

By artificially suppressing different terms, we study the linear drive of the dominant instabilities. For the DK model, the peak growth rate at low k_{\parallel} is a Kelvin-Helmholz instability D'Angelo (1965). More specifically, the modes are driven by the $[\phi_{DK}, \Omega]$ and the $[\nabla_{\perp} \phi_{DK}, \omega]$ terms in Eq. (5.14e). This finding is consistent with previous long-wavelength simulations of linear plasma devices Frei *et al.* (2024); Mencke & Ricci (2025); Rogers & Ricci (2010).

For the GK model, the dominant instability is at $k_{\parallel} = 0.87/R$ and $m = 5$ and it is driven by the $[\phi_{DK}, \mathcal{N}_{iGK}^{pj}]$ term in Eq. (4.4a) for $p = j = 0$. It is driven by shear flow and a density gradient since both the GK density gradient and the gradient of the DK electrostatic potential are necessary for the instability to appear. We note that for $m = 5$, using Eq. (4.5), $\mathcal{C}_{ii}^{00} \sim -0.051\nu_{i0}\tau_i\mathcal{N}_{iGK}^{00}$. Therefore, collisions damp this instability with $\gamma \sim 0.036c_{s0}/R$ when using the physical collisionality.

The dominant instability for the full model is a Kelvin-Helmholz mode with the growth rate enhanced by the $[\phi_{DK}, \mathcal{N}_{iGK}^{pj}]$ term in Eq. (4.4a) for $p = j = 0$ and the $[\phi_{GK}, \mathcal{N}_{iDK}^{pj}]$ term in Eq. (3.12a) for $p = j = 0$. Through a DK density gradient, the Kelvin-Helmholz mode is coupled to the GK fields. We note that $\bar{\phi}_{GK}$ is an order of magnitude smaller than the amplitude of $\bar{\phi}_{DK}$. Therefore, we do not observe a significant influence of $\bar{\phi}_{GK}$ in the 1D linear simulations.

In order to study the development of small-scale structures observed for the low-collisionality and larger-GK-sources simulations observed in Fig. 8, we assume that $k_{\parallel} = 0$, F_{iDK} is a Maxwellian constant in time and space, and F_{iGK} is an isotropic Maxwellian. Focusing on a small gradient region with a gradient length of $x_0 < \rho_{s0}$, and assuming that $|\nabla_{\perp} \phi_{GK}| \sim \frac{T_e}{eN_e} |\nabla_{\perp} \varrho_i^*| \gg |\nabla_{\perp} \phi_{DK}|$, we obtain the following condition for an instability,

$$\frac{1}{T_{eDK}} + \frac{1}{T_i} \left[1 - \exp\left(-\frac{T_{iDK}k_{\perp}^2}{\Omega_i^2}\right) I_0\left(\frac{T_{iDK}k_{\perp}^2}{\Omega_i^2}\right) \right] > \frac{|\nabla_{\perp} \varrho_i^*|}{eN_{DK}|\nabla_{\perp} \phi_{GK}|}. \quad (8.3)$$

The details of the calculation leading to Eq. (8.3) are specified in App. C. For small structures where $v_{Thi}k_{\perp} \gg \Omega_i$, we expect $\phi_{GK} \sim T_{eDK}\varrho_i^*/N_{DK}$. Indeed, in Eq. (5.16), using Eqs. (B 1a) and (B 1b) $\left\| \partial_{\mu} \langle \langle \phi_{GK} \rangle_{\mathbf{R}} \rangle_{\mathbf{x}}^{\dagger} \right\| \propto \exp(-T_{i0}k_{\perp}^2/m_i\Omega_i^2) \rightarrow 0$ when $v_{Thi}k_{\perp} \gg \Omega_i$. Therefore, Eq. (8.3) is in general satisfied for large enough k_{\perp} . This instability would allow for a non-linear growth of small-scale structures (due to the gradient size, x_0 , of ϕ_{GK} further decreasing). On the other hand, the $\sim \nu_{i0}\nabla_{\perp}^2$ term in Eq. (4.5) and the

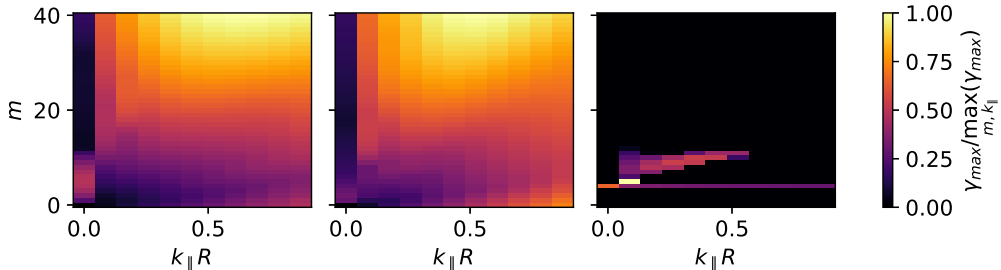


FIGURE 12. The linear growth rates of the system of Eqs. (3.5a), (3.5b) (5.14e), (5.14g), (5.15b), (5.8b), and (5.16) with $(P_{DK}, J_{DK}, P_{GK}, J_{GK}) = (4, 2, 4, 3)$, for the full system (left), for the DK system with $f_{GK} = 0$ (center), and for the GK system with $\tilde{f}_{DK} = 0$ (right), $r_g = 22\rho_{s0}$. The simulations with physical GK collisionality and sources are used to calculate the equilibrium fields for the DK system while the simulations with ν_{i0} in Eq. (4.5) reduced by a factor of 1000 and with A_E and A_N increased by a factor 10 in Eq. (6.4c) are used for the two other systems. The maximum growth rates for the full model is $\max_{m, k_{\parallel}}(\gamma_{max}) = 0.59c_{s0}/R$, for the DK model it is $\max_{m, k_{\parallel}}(\gamma_{max}) = 0.38c_{s0}/R$ and for the GK model it is $\max_{m, k_{\parallel}}(\gamma_{max}) = 0.014c_{s0}/R$. The highest growth rate for the full system is observed at $m = 40$ and $k_{\parallel} \sim 0.61/R$.

$\exp\left(-\frac{T_{i0}k_{\parallel}^2}{\Omega_i^2}\right)$ factor in ϱ_i^* in Eq. (B 1b) inhibits the buildup of large gradient regions for ϕ_{GK} . As a direct consequence, in the global simulations, this instability is only observed in the simulation with low GK collisionality.

9. Conclusion

First of a kind simulations that self-consistently couple full-f drift-kinetic (DK) and δ -f gyrokinetic (GK) fields are performed in a linear plasma device, relying on a gyromoment approach. We consistently derive the ion and electron system of equations starting from the gyro-averaged Boltzmann equations. Adopting a critical balance ordering, we find that the electrons are described by a drift-reduced Braginskii model. The DK and GK parts of the ion distribution function are projected on a Hermite-Laguerre basis yielding a hierarchy equation for the resulting gyromoments of the distribution function.

The physical model is numerically implemented and simulations are carried out using LAPD parameters. Spectral convergence is observed with a small amount of moments, due to the high ion-ion collisionality that leads to an ion distribution function close to a bi-Maxwellian. The inclusion of the small-scale GK part of the electrostatic potential and ion gyromoments does not affect the DK fields at the physical collisionality. When artificially reducing the GK collision term and increasing the GK sources, a small increase

in small-scale turbulent structures in the plane perpendicular to the magnetic field is observed for the DK fields.

The GK electrostatic potential is dominated by long-wavelength modes that have significantly smaller perpendicular sizes than its DK counterpart as well as smaller amplitude satisfying the assumptions behind the physical model. The amplitude of the GK gyromoments quickly decreases with increasing order of the Hermite and Laguerre polynomials due to the high ion-ion collisionality.

Linearly, the growth-rates of the system of equations are driven by the DK fields supporting the findings from the global full-f simulations that the GK fields play a subdominant role in driving turbulence. The driving instability has a Kelvin-Helmholz nature. If the amplitude of the GK sources are amplified and collisions for the GK fields are suppressed, increased growth rates are observed caused by the GK density gradients. In this scenario, the growth rate of unstable modes at large perpendicular wavenumbers is amplified. We show analytically that small gradient length scales for the GK potential and density can drive a GK Kelvin-Helmholz-like instability. Additionally, this instability can non-linearly cause small-scale structures to develop in the full 3D simulations.

Acknowledgements

The authors thank, Louis N. Stenger, Brenno Jason Sanzio Peter De Lucca, Samuel Ernst, and Zeno Tecchiolli for fruitful discussions. Simulations were carried out due to the grant EHPC-REG-2023R03-144 on the Discoverer supercomputer. This work has been carried out within the framework of the EUROfusion Consortium, partially funded by the European Union via the Euratom Research and Training Programme (Grant Agreement No 101052200 — EUROfusion). The Swiss contribution to this work has been funded in part by the Swiss State Secretariat for Education, Research and Innovation (SERI). Views and opinions expressed are however those of the author(s) only and do not necessarily reflect those of the European Union, the European Commission or SERI. Neither the European Union nor the European Commission nor SERI can be held responsible for them.

REFERENCES

ARAKAWA, A. 1997 Computational design for long-term numerical integration of the equations

- of fluid motion: Two-dimensional incompressible flow. Part I. *Journal of computational physics* **135** (2), 103.
- BALAY, SATISH, ABHYANKAR, SHRIRANG, ADAMS, MARK F., BENSON, STEVEN, BROWN, JED, BRUNE, PETER, BUSCHELMAN, KRIS, CONSTANTINESCU, EMIL M., DALCIN, LISANDRO, DENER, ALP, EIJKHOUT, VICTOR, FAIBUSSOWITSCH, JACOB, GROPP, WILLIAM D., HAPLA, VÁCLAV, ISAAC, TOBIN, JOLIVET, PIERRE, KARPEEV, DMITRY, KAUSHIK, DINESH, KNEPLEY, MATTHEW G., KONG, FANDE, KRUGER, SCOTT, MAY, DAVE A., MCINNES, LOIS CURFMAN, MILLS, RICHARD TRAN, MITCHELL, LAWRENCE, MUNSON, TODD, ROMAN, JOSE E., RUPP, KARL, SANAN, PATRICK, SARICH, JASON, SMITH, BARRY F., ZAMPINI, STEFANO, ZHANG, HONG, ZHANG, HONG & ZHANG, JUNCHAO 2024 PETSc Web page. <https://petsc.org/>.
- BEER, M. A. & HAMMETT, G. W. 1996 Toroidal gyrofluid equations for simulations of tokamak turbulence. *Physics of Plasmas* **3** (11), 4046.
- BRAGINSKII, SI 1965 Transport processes in a plasma. *Reviews of plasma physics* **1**, 205.
- CHANG, C. S., KU, S., LOARTE, A., PARAIL, V., KOECHL, F., ROMANELLI, M., MAINGI, R., AHN, J.-W., GRAY, T., HUGHES, J. & OTHERS 2017 Gyrokinetic projection of the divertor heat-flux width from present tokamaks to ITER. *Nuclear Fusion* **57** (11), 116023.
- D'ANGELO, NICOLA 1965 Kelvin—helmholtz instability in a fully ionized plasma in a magnetic field. *The Physics of Fluids* **8** (9), 1748–1750.
- DORF, M. & DORR, M. 2020 Progress with the 5D full-F continuum gyrokinetic code COGENT. *Contributions to Plasma Physics* **60** (5), e201900113.
- DOUGHERTY, J. P. 1964 Model Fokker-Planck equation for a plasma and its solution. *The Physics of Fluids* **7** (11), 1788.
- FREI, B. J., JORGE, R. & RICCI, P. 2020 A gyrokinetic model for the plasma periphery of tokamak devices. *Journal of Plasma Physics* **86** (2), 905860205.
- FREI, B. J., MENCKE, J & RICCI, P 2024 Full-f turbulent simulation in a linear plasma device using a gyro-moment approach. *Physics of Plasmas* **31** (1).
- FRIEDMAN, B., CARTER, T. A., UMANSKY, M. V., SCHAFFNER, D. & DUDSON, B. 2012 Energy dynamics in a simulation of lapd turbulence. *Physics of Plasmas* **19** (10), 102307.
- FRIGO, MATTEO & JOHNSON, STEVEN G. 2005 The design and implementation of FFTW3. *Proceedings of the IEEE* **93** (2), 216–231, special issue on “Program Generation, Optimization, and Platform Adaptation”.
- GEKELMAN, W., PFISTER, H., LUCKY, Z., BAMBER, J., LENEMAN, D. & MAGGS, J. 1991 Design, construction, and properties of the large plasma research device- The LAPD at UCLA. *Review of scientific instruments* **62** (12), 2875.
- GIACOMIN, M., RICCI, P., COROADO, A., FOURESTEY, G., GALASSI, D., LANTI, E., MANCINI, D., RICHART, N., STENGER, L. N. & VARINI, N. 2022 The gbs code for the self-consistent simulation of plasma turbulence and kinetic neutral dynamics in the tokamak boundary. *Journal of Computational Physics* p. 111294.

- HAHM, TS, WANG, LU & MADSEN, JENS 2009 Fully electromagnetic nonlinear gyrokinetic equations for tokamak edge turbulence. *Physics of Plasmas* **16** (2).
- HAKIM, A. H., MANDELL, N. R., BERNARD, T. N., FRANCISQUEZ, M., HAMMETT, G. W. & SHI, E. L. 2020 Continuum electromagnetic gyrokinetic simulations of turbulence in the tokamak scrape-off layer and laboratory devices. *Physics of Plasmas* **27** (4), 042304.
- HELD, MARKUS & WIESENBERGER, MATTHIAS 2022 Beyond the oberbeck–boussinesq and long wavelength approximation. *Nuclear Fusion* **63** (2), 026008.
- HELD, MARKUS, WIESENBERGER, MATTHIAS & KENDL, ALEXANDER 2020 Padé-based arbitrary wavelength polarization closures for full-f gyro-kinetic and-fluid models. *Nuclear Fusion* **60** (6), 066014.
- HOFFMANN, A. C. D., FREI, B. J. & RICCI, P. 2023a Dimits shift and impact of collisions using a gyrokinetic moment-based approach. *arXiv preprint arXiv:2308.01016* .
- HOFFMANN, A. C. D., FREI, B. J. & RICCI, P. 2023b Gyrokinetic simulations of plasma turbulence in a z-pinch using a moment-based approach and advanced collision operators. *Journal of Plasma Physics* **89** (2), 905890214.
- JENKO, FRANK, DORLAND, W, KOTSCHENREUTHER, M & ROGERS, BN 2000 Electron temperature gradient driven turbulence. *Physics of plasmas* **7** (5), 1904–1910.
- KAUFMAN, ALLAN N 1986 The electric dipole of a guiding center and the plasma momentum density. *The Physics of fluids* **29** (5), 1736–1737.
- LOIZU, J., RICCI, P., HALPERN, F. D. & JOLLIET, S. 2012 Boundary conditions for plasma fluid models at the magnetic presheath entrance. *Physics of Plasmas* **19** (12), 122307.
- MANDELL, N., DORLAND, W., ABEL, I., GAUR, R., KIM, P., MARTIN, M. & QIAN, T. 2022 GX: a GPU-native gyrokinetic turbulence code for tokamaks and stellarators. *arXiv:2209.06731* .
- MENCKE, JE & RICCI, P 2025 Extended drift-kinetic full-f turbulent simulation of a linear plasma device using the gyro-moment approach. *Plasma Physics and Controlled Fusion* **67** (3), 035029.
- MICHELS, D., ULBL, P., ZHOLOBENKO, W., BODY, T., STEGMEIR, A., EICH, T., GRIENER, M., CONWAY, G. D., JENKO, F. & TEAM, ASDEX UPGRADE 2022 Full-f electromagnetic gyrokinetic turbulence simulations of the edge and scrape-off layer of ASDEX Upgrade with GENE-X. *Physics of Plasmas* **29** (3), 032307.
- MOSETTO, A., HALPERN, F. D., JOLLIET, S., LOIZU, J. & RICCI, P. 2015 Finite ion temperature effects on scrape-off layer turbulence. *Physics of Plasmas* **22** (1), 012308.
- ORSZAG, STEVEN A 1971 On the elimination of aliasing in finite-difference schemes by filtering high-wavenumber components. *Journal of Atmospheric Sciences* **28** (6), 1074–1074.
- PAN, Q., TOLD, D. & JENKO, F. 2016 Fully nonlinear δf gyrokinetics for scrape-off layer parallel transport. *Physics of Plasmas* **23** (10), 102302.
- PAN, Q., TOLD, D., SHI, E., HAMMETT, G. W. & JENKO, F. 2018 Full-f version of GENE for turbulence in open-field-line systems. *Physics of Plasmas* **062303** (25), 1.

- PARRA, FELIX 2019 Lecture notes on *Braginskii fluid equations*.
- PARUTA, P., RICCI, P., RIVA, F., WERSAL, C., BEADLE, C. & FREI, B. 2018 Simulation of plasma turbulence in the periphery of diverted tokamak by using the GBS code. *Physics of Plasmas* **25** (11), 112301.
- PFIRSCH, DIETER & MORRISON, PHILIP J 1985 Local conservation laws for the maxwell-vaslov and collisionless kinetic guiding-center theories. *Physical Review A* **32** (3), 1714.
- POPOVICH, P., UMANSKY, M. V., CARTER, T. A. & FRIEDMAN, B. 2010 Analysis of plasma instabilities and verification of the bout code for the large plasma device. *Physics of Plasmas* **17** (10), 102107.
- PRESS, WH, TEUKOLSKY, SA, VETTERING, WT & FLANNERY, BP 1992 *Numerical Recipes in Fortran, The Art of Scientific Computing*. Cambridge University Press.
- QIN, H, COHEN, RH, NEVINS, WM & XU, XQ 2006 General gyrokinetic equations for edge plasmas. *Contributions to Plasma Physics* **46** (7-9), 477–489.
- ROGERS, B. N. & RICCI, P. 2010 Low-frequency turbulence in a linear magnetized plasma. *Physical Review Letters* **104** (22), 225002.
- SHI, E. L., HAMMETT, G. W., STOLTZFUS-DUECK, T. & HAKIM, A. 2017 Gyrokinetic continuum simulation of turbulence in a straight open-field-line plasma. *Journal of Plasma Physics* **83** (3), 905830304.
- ULBL, P., BODY, T., ZHOLOBENKO, W., STEGMEIR, A., PFENNIG, J. & JENKO, F. 2023 Influence of collisions on the validation of global gyrokinetic simulations in the edge and scrape-off layer of TCV. *Physics of Plasmas* **30** (5).
- WIESENBERGER, MATTHIAS & HELD, MARKUS 2022 Long-wavelength closures for collisional and neutral interaction terms in gyro-fluid models. In *Journal of Physics: Conference Series*, , vol. 2397, p. 012015. IOP Publishing.
- WIESENBERGER, M & HELD, M 2023 Effects of plasma resistivity in three-dimensional full- f gyro-fluid turbulence simulations. *arXiv preprint arXiv:2309.10414* .
- ZEILER, A., DRAKE, J. F. & ROGERS, B. 1997 Nonlinear reduced braginskii equations with ion thermal dynamics in toroidal plasma. *Physics of Plasmas* **4** (6), 2134.

Appendix A. Calculation of higher order electron distribution function

In order to solve for F_{eDK1} , we use the ansatz Eq. (3.4a) with the additional ansatz for f_{sh} in Eq. (3.4b). We project Eq. (3.3) on the $v_{\parallel} L_j^{(3/2)}$ basis, using parity in v_{\parallel} (notice

that the collision operators conserve parity in \mathbf{v})

$$\frac{4}{3\sqrt{\pi}} \left(2\Gamma(5/2) \delta_0^j (\nabla_{\parallel} P_{e1} + eN_{e1} \nabla_{\parallel} \phi_{DK}) - 2\Gamma(7/2) \delta_1^j \left(\nabla_{\parallel} P_{e1} + e \frac{P_{e1}}{T_0} \nabla_{\parallel} \phi_{DK} \right) \right) = m_e (C_{ee1}^j + C_{ei1}^j) \quad (\text{A } 1a)$$

$$C_{ee1}^j = v_{The}^2 \nu_{ee} \sum_p K_{ee}^{jp} A_p, \quad (\text{A } 1b)$$

$$C_{ei1}^j = v_{The}^2 \nu_{ei} \left(\sum_p K_{ei}^{jp} A_p - \frac{m_e}{T_{e0}} K_{ei}^{j0} J_{\parallel} \right), \quad (\text{A } 1c)$$

and finally,

$$\delta_0^j (\nabla_{\parallel} P_{e1} + eN_{e1} \nabla_{\parallel} \phi_{DK}) + m_e \nu_{ei} K_{ei}^{j0} J_{\parallel} - \frac{5}{2} \delta_1^j \left(\nabla_{\parallel} P_{e1} + e \frac{P_{e1}}{T_{e0}} \nabla_{\parallel} \phi_{DK} \right) = T_{e0} \sum_k \left(\nu_{ee} K_{ee}^{jk} + \nu_{ei} K_{ei}^{jk} \right) A_k, \quad (\text{A } 1d)$$

where we have defined Braginskii (1965); Parra (2019)

$$\begin{pmatrix} K_{ee}^{00} & K_{ee}^{01} & K_{ee}^{02} & K_{ee}^{03} & \dots \\ K_{ee}^{10} & K_{ee}^{11} & K_{ee}^{12} & K_{ee}^{13} & \dots \\ K_{ee}^{20} & K_{ee}^{21} & K_{ee}^{22} & K_{ee}^{23} & \dots \\ K_{ee}^{30} & K_{ee}^{31} & K_{ee}^{32} & K_{ee}^{33} & \dots \\ \vdots & \vdots & \vdots & \vdots & \ddots \end{pmatrix} = \sqrt{2} \begin{pmatrix} 0 & 0 & 0 & 0 & \dots \\ 0 & 1 & 3/4 & 15/32 & \dots \\ 0 & 3/4 & 45/16 & 309/128 & \dots \\ 0 & 15/32 & 309/128 & 5657/1024 & \dots \\ \vdots & \vdots & \vdots & \vdots & \ddots \end{pmatrix}, \quad (\text{A } 2a)$$

$$\begin{pmatrix} K_{ei}^{00} & K_{ei}^{01} & K_{ei}^{02} & K_{ei}^{03} & \dots \\ K_{ei}^{10} & K_{ei}^{11} & K_{ei}^{12} & K_{ei}^{13} & \dots \\ K_{ei}^{20} & K_{ei}^{21} & K_{ei}^{22} & K_{ei}^{23} & \dots \\ K_{ei}^{30} & K_{ei}^{31} & K_{ei}^{32} & K_{ei}^{33} & \dots \\ \vdots & \vdots & \vdots & \vdots & \ddots \end{pmatrix} = \begin{pmatrix} 1 & 3/2 & 15/8 & 35/16 & \dots \\ 3/2 & 13/4 & 69/16 & 165/32 & \dots \\ 15/8 & 69/16 & 433/64 & 1077/128 & \dots \\ 35/16 & 165/32 & 1077/128 & 2957/256 & \dots \\ \vdots & \vdots & \vdots & \vdots & \ddots \end{pmatrix}. \quad (\text{A } 2b)$$

We note that the $j = 0$ equation of Eq. (A 1d) is solved for using $J_{\parallel} = \mathcal{O}(c_s n_e \epsilon_{\perp})$ which gives the additional condition by combining Eq. (3.10a) with $(p, j) = (1, 0)$ and Eq. (A 1d) with $j = 0$,

$$\frac{1}{m_i} \nabla_{\parallel} P_{\parallel i DK} - \frac{1}{m_e} \nabla_{\parallel} P_{e1} - \frac{eN_{e1}}{m_e} \nabla_{\parallel} \phi_{DK} = \nu_{ei} \left(J_{\parallel} - \frac{T_{e0}}{m_e} \sum_k K_{ei}^{0k} A_k \right) + \mathcal{O}(\Omega_i c_s \epsilon_{\perp}^2). \quad (\text{A } 3)$$

We obtain from Eq. (A 1d) the following system,

$$\sum_k \left(K_{ee}^{jk} + K_{ei}^{jk} \right) A_k = \begin{bmatrix} C_{P1} \\ 0 \\ 0 \end{bmatrix} + \frac{m_e n_e}{T_e} U_{\parallel iDK} K_{ei}^{j0}, \quad (\text{A } 4)$$

with

$$C_{P1} = \frac{1}{T_{e0} \nu_{ee}} \left(\nabla_{\parallel} P_{e1} + e \frac{P_{e1}}{T_{e0}} \nabla_{\parallel} \phi_{DK} \right) = \frac{N_{e0}}{T_{e0} \nu_{ee}} \nabla_{\parallel} T_{e1}, \quad (\text{A } 5)$$

where we have defined $T_{e1} = P_{e1}/N_{e0}$ and used Eq. (3.2b) to relate $\nabla_{\parallel} \phi_{DK}$ to $\nabla_{\parallel} N_{e0}$.

The solution to Eq. (A 4) truncated at $j = 3$ gives Braginskii (1965); Parra (2019)

$$A_1 = 1.266 C_{P1} + 0.286 \frac{m_e}{T_{e0}} J_{\parallel}, \quad (\text{A } 6a)$$

$$A_2 = -0.654 C_{P1} + 0.055 \frac{m_e}{T_{e0}} J_{\parallel}, \quad (\text{A } 6b)$$

$$A_3 = 0.0193 C_{P1} + 0.0238 \frac{m_e}{T_{e0}} J_{\parallel}. \quad (\text{A } 6c)$$

Taking the moments of Eq. (3.3) with 1, and $m_e v^2$ gives

$$\partial_t N_{e0} + \frac{1}{B} [\phi_{DK} + \phi_{GK}, N_{e0}] + \nabla_{\parallel} (N_{e0} U_{\parallel iDK} - J_{\parallel}) = S_N, \quad (\text{A } 7a)$$

$$\begin{aligned} & 3\partial_t T_{e1} + \frac{3}{B} [\phi_{DK} + \phi_{GK}, T_{e0}] + \frac{2}{N_{e0}} \nabla_{\parallel} q_{\parallel e} \\ & - 2U_{\parallel eDK} \frac{T_{e0}}{N_{e0}} \nabla_{\parallel} n_e - 3 \frac{T_{e0}}{N_{e0}} \nabla_{\parallel} (N_{e0} U_{\parallel eDK}) = \mathcal{C}_{ei1}^{mv^2} + 2 \frac{S_{Pe}}{N_{e0}} - 3 \frac{T_{e0}}{N_{e0}} S_n, \end{aligned} \quad (\text{A } 7b)$$

$$\begin{aligned} & 3\partial_t T_{e0} + \frac{3}{B} [\phi_{DK} + \phi_{GK}, T_{e0}] + \frac{1}{N_{e0}} \nabla_{\parallel} (2q_{\parallel e} + 3T_{e0} J_{\parallel}) \\ & - 2U_{\parallel iDK} \frac{T_{e0}}{N_{e0}} \nabla_{\parallel} N_{e0} + 2J_{\parallel} \frac{T_{e0}}{N_{e0}^2} \nabla_{\parallel} N_{e0} - 3 \frac{T_{e0}}{N_{e0}} \nabla_{\parallel} (N_{e0} U_{\parallel iDK}) = \mathcal{C}_{ei1}^{mv^2} + 2 \frac{S_{Pe}}{N_{e0}} - 3 \frac{T_{e0}}{N_{e0}} S_n, \end{aligned} \quad (\text{A } 7c)$$

with

$$q_{\parallel e} = \frac{1}{2} \int d\mathbf{v} m_e v_{\parallel} v^2 F_{e1} = T_{e0} \left(\frac{5}{2} N_{e0} U_{\parallel eDK} - \frac{5}{2} \frac{A_1}{m_e} \right), \quad (\text{A } 7d)$$

$\|S_e\|_e = S_N$, $\|m_e v^2 S_e/2\|_e = S_{Pe}$, and $\|m_e v^2 C_{ei}/2\|_e = \mathcal{C}_{ei1}^{mv^2}$.

Finally, we define $N_{eDK} = N_{e0} + N_{e1}$ and $T_{eDK} = T_{e0} + T_{e1}$, neglecting $\mathcal{C}_{ei1}^{mv^2}$ and adding a few terms to Eqs. (A 7a) and (A 7c) noticing that these does not change the order of validity regime of the equations, we arrive at Eqs. (3.5a) and (3.5b) having defined $S_{T_e} = S_{Pe}/3N_{eDK} - T_{eDK} S_N/N_{eDK}$. It is noted that Eqs. (A 7a) and (A 7c) have some

higher order terms, however, these are added such that they exactly correspond to the drift-reduced-Braginskii model Parra (2019); Zeiler *et al.* (1997).

Equation (A3) represents nothing more than force balance for electrons and ions. In order to maintain quasi neutrality, we need $J_{\parallel} \sim 0$ which for large ν_{ei} is obviously satisfied. For low ν_{ei} , if there is an imbalance in the accelerations from the electron and ion pressure, a large electric field builds up to accelerate the electrons such that $U_{\parallel e} \sim U_{\parallel i}$.

Appendix B. Hermite-Laguerre projection of gyroaveraged quantities

For completeness, the complicated expression for the gyroaveraged quantities in Eqs. (4.4a) and (5.16) are reported. The linear expressions (in ϕ_{GK}) are given by Frei *et al.* (2020)

$$\begin{aligned} \left\| \partial_{\mu} \langle \langle \phi_{GK} \rangle_{\mathbf{R}} \rangle_{\mathbf{x}}^{\dagger} \right\|_i &= - \sum_{\mathbf{k}} \frac{B}{T_{i0}} \sum_{n \geq 0, m \geq 1} K_n(b_i) K_m(b_i) \\ &\times \sum_{l=0}^{m-1} \sum_{f=0}^{n+l} \bar{d}_{nlf}^0 \mathcal{N}_{iDK}^{0f} \phi_{GK}(\mathbf{k}) e^{i\mathbf{k} \cdot \mathbf{x}}, \end{aligned} \quad (\text{B1a})$$

$$\varrho_i^* = \sum_{\mathbf{k}} \sum_{n \geq 0} K_n(b_i) \mathcal{N}_{iGK}^{0n}(\mathbf{k}) e^{i\mathbf{k} \cdot \mathbf{x}}, \quad (\text{B1b})$$

$$\| \langle \phi_{GK} \rangle_{\mathbf{R}} \|_i^{pj} = \sum_{\mathbf{k}} \sum_{n \geq 0} D_n^{pjn} \phi_{GK}(\mathbf{k}) e^{i\mathbf{k} \cdot \mathbf{R}}, \quad (\text{B1c})$$

$$D_n^{pkl} = \sum_{r=0}^{l+k} \bar{d}_{lkr}^0 \mathcal{N}_{iDK}^{pr} K_n(b_i), \quad (\text{B1d})$$

$$\bar{d}_{rjf}^n = \sum_{r_1=0}^r \sum_{j_1=0}^j \sum_{f_1=0}^f L_{jj_1}^{-1/2} L_{rr_1}^{n-1/2} L_{ff_1}^{-1/2} (r_1 + j_1 + f_1)!, \quad (\text{B1e})$$

$$L_{nl}^m = \frac{(-1)^l (m+n+1/2)!}{(n-l)! (m+l+1/2)! l!}, \quad (\text{B1f})$$

$$K_n(b_i) = \frac{1}{n!} \left(\frac{b_i}{2} \right)^{2n} e^{-(b_i/2)^2}, \quad b_i = \frac{k_{\perp} \sqrt{2T_{i0}}}{\Omega_i \sqrt{m_i}}, \quad (\text{B1g})$$

while the non-linear projections are

$$\begin{aligned} \|\langle \psi \rangle_{\mathbf{R}} - \langle \phi_{GK} \rangle_{\mathbf{R}}\|_i^{pj} &= \frac{q_i^2}{2m_i \Omega_i} \left\| \partial_\mu \left(\langle \phi_{GK} \rangle_{\mathbf{R}}^2 - \langle \phi_{GK}^2 \rangle_{\mathbf{R}} \right) \right\|_i^{pj} \\ &+ \frac{q_i}{2m_i \Omega_i^2} \left\| \left\langle \left(\mathbf{b} \times \nabla \widetilde{\phi_{GK}} \right) \cdot \nabla \widetilde{\phi_{GK}} \right\rangle_{\mathbf{R}} \right\|_i^{pj}, \end{aligned} \quad (\text{B } 1h)$$

$$\begin{aligned} \left\| \partial_\mu \left(\langle \phi_{GK} \rangle_{\mathbf{R}}^2 - \langle \phi_{GK}^2 \rangle_{\mathbf{R}} \right) \right\|_i^{pj} &= \sum_{\mathbf{k}, \mathbf{k}'} \sum_{n=0}^{\infty} \frac{1}{n+1} \left[K_n(|\mathbf{b}_i + \mathbf{b}'_i|) |\mathbf{k}_\perp + \mathbf{k}'_\perp|^2 \sum_{f=0}^{j+n} d_{nmf}^1 \mathcal{N}_{iDK}^{pj} \right. \\ &- \sum_{m=0}^{\infty} \left(K_n(b_i) K_m(b'_i) k_\perp^2 + K_n(b'_i) K_m(b_i) (k'_\perp)^2 \right) \\ &\left. \sum_{f=0}^{m+n} d_{nmf}^1 \sum_{s=0}^{f+j} d_{fjs}^0 \mathcal{N}_{iDK}^{ps} \right] \phi_{GK}(\mathbf{k}) \phi_{GK}(\mathbf{k}') e^{i(\mathbf{k}+\mathbf{k}') \cdot \mathbf{R}}, \end{aligned} \quad (\text{B } 1i)$$

while the final term is a bit more tricky, without projecting, it can be expressed as

$$\begin{aligned} \left\langle \left(\mathbf{b} \times \nabla \widetilde{\phi_{GK}} \right) \cdot \nabla \widetilde{\phi_{GK}} \right\rangle_{\mathbf{R}} &= 2 \sum_{\mathbf{k}, \mathbf{k}', n > 0} \mathbf{b} \times \mathbf{k} \cdot \mathbf{k}' \frac{(-1)^n}{n} J_n(b') J_n(b) \sin n\alpha \\ &\phi_{GK}(\mathbf{k}) \phi_{GK}(\mathbf{k}') e^{i(\mathbf{k}+\mathbf{k}') \cdot \mathbf{R}}, \end{aligned} \quad (\text{B } 2)$$

where we have introduced α as the angle between \mathbf{k} and \mathbf{k}' such that $\mathbf{k} \cdot \mathbf{k}' = kk' \cos \alpha$ and the Bessel function of the first kind of order n , J_n . Finally we truncate the sum in Eq. (B 2) at $n = 1$ for simplicity and get

$$\begin{aligned} \left\| \left\langle \left(\mathbf{b} \times \nabla \widetilde{\phi_{GK}} \right) \cdot \nabla \widetilde{\phi_{GK}} \right\rangle_{\mathbf{R}} \right\|_i^{pj} &= \frac{T_{i0}}{m_i \Omega_i^2} (\mathbf{b} \times \mathbf{k} \cdot \mathbf{k}')^2 \sum_{n=0}^{\infty} \sum_{m=0}^{\infty} \frac{1}{(n+1)} K_n(b_i) K_m(b'_i) \\ &\times \left(\sum_{f=0}^{m+n} d_{nmf}^1 - \sum_{f=0}^{m+1+n} d_{n(m+1)f}^1 \right) \sum_{s=0}^{f+j} d_{fjs}^0 \mathcal{N}_{iDK}^{ps} \phi_{GK}(\mathbf{k}) \phi_{GK}(\mathbf{k}') e^{i(\mathbf{k}+\mathbf{k}') \cdot \mathbf{R}}. \end{aligned} \quad (\text{B } 3)$$

Finally for the projection on the GK distribution function, we simply replace \mathcal{N}_{iDK}^{pj} with \mathcal{N}_{iGK}^{pj} in Eq. (B 1c). For all the sums, we truncate maximally at J_{DK} and J_{GK} for the DK and GK projections, respectively Hoffmann *et al.* (2023b,a).

Appendix C. Linear dispersion relation of the GK Kelvin-Helmholz mode

In this appendix, we derive a dispersion relation for the $k_{\parallel} = 0$, $m \gg 1$ mode observed for the full model in Fig. 12. We go to a slab geometry with x the radial direction and y the poloidal direction. We assume that the ion DK distribution function is a fixed Maxwellian with density N_{DK} and temperature T_i , furthermore, we approximate the ion

GK distribution function as an isotropic distribution function, also, with temperature T_i . We linearize all fields, f , with the equilibrium $\bar{f} = \bar{f}(x)$ and the fluctuating part $\tilde{f}(x) \exp(-i\omega t + ik_y y)$. We use Eq. (5.14e), perform the gyroaverage operation on Eq. (4.4a) with $(p, j) = (0, 0)$ while only including terms linear in ϵ_δ . Finally, we close the system with Eq. (5.16) and to get

$$\nabla_\perp \cdot \left(-i\omega^* N_{DK}^- \nabla_\perp \phi_{DK}^- - ik_y^* N_{DK}^- \partial_x \nabla_\perp \phi_{DK}^- \phi_{tot}^- \right) = 0, \quad (\text{C1a})$$

$$-i\omega \tilde{\varrho}_i^* + ik_y^* \left(\partial_x \phi_{DK}^- \tilde{\varrho}_i^* - \partial_x \tilde{\varrho}_i^* \phi_{DK}^- \right) = 0, \quad (\text{C1b})$$

$$\tilde{\varrho}_i^* = N_{DK}^- I_y \phi_{GK}^-, \quad (\text{C1c})$$

with

$$I_y = e \left(\frac{1}{T_e} + \frac{1}{T_i} - \frac{1}{T_i} \exp \left(-\frac{b_{iy}^2}{2} \right) I_0 \left(\frac{b_{iy}^2}{2} \right) \right), \quad (\text{C1d})$$

$$k_y^* = \frac{k_y}{B\rho_*}, \quad \phi_{tot} = \phi_{DK} + \phi_{GK}, \quad \text{and} \quad \omega^* = \omega - k_y^* \partial_x \phi_{tot}^-. \quad (\text{C1e})$$

Neglecting the long-wavelength contribution of Eq. (C1a), i.e. only keeping terms linear in ϕ_{GK} and combining the equations lead to

$$-\nabla_\perp \cdot \left(k_y^* \partial_x \phi_{GK}^- \nabla_\perp \phi_{DK}^- + \frac{(k_y^*)^2}{(\omega - k_y^* \partial_x \phi_{DK}^-) I_y} \partial_x \nabla_\perp \phi_{DK}^- \partial_x \tilde{\varrho}_i^* \phi_{DK}^- \right) = 0. \quad (\text{C2})$$

Assuming that $\partial_x \phi_{DK}$ and $\partial_x \phi_{GK}$ are piecewise linear around a region of x_0

$$\partial_x \phi_{DK}^- = \begin{cases} -V_0, & x < -x_0, \\ V_0 \frac{x}{x_0}, & -x_0 < x < x_0, \\ V_0, & x > x_0, \end{cases}, \quad (\text{C3a})$$

$$\partial_x \phi_{GK}^- = \begin{cases} -V_1, & x < -x_0, \\ V_1 \frac{x}{x_0}, & -x_0 < x < x_0, \\ V_1, & x > x_0, \end{cases}, \quad (\text{C3b})$$

while $\phi_{DK}^- = V_n$ is constant. We assume that $V_0 \ll V_1$ such that a general solution for ϕ_{DK}^- is

$$\phi_{DK}^- = \begin{cases} (A_1 + A_2 \exp(2k_y x_0)) \exp(k_y x), & x < -x_0, \\ A_1 \exp(k_y x) + A_2 \exp(-k_y x), & -x_0 < x < x_0, \\ (A_2 + A_1 \exp(2k_y x_0)) \exp(-k_y x), & x > x_0, \end{cases} \quad (\text{C4})$$

where we have used that ϕ_{DK}^{\sim} vanishes at $-\infty$ and ∞ and is continuous. Finally, we integrate Eq. (C2) over each discontinuity ($x = \pm x_0$) and obtain a matching condition

$$\begin{bmatrix} \frac{(k_y^*)^2 V_0 V_n}{(\omega + k_y^* V_0) x_0 I_y} e^{-2k_y x_0} & -2k_y k_y^* V_1 + \frac{(k_y^*)^2 V_0 V_n}{(\omega + k_y^* V_0) x_0 I_y} \\ 2k_y k_y^* V_1 + \frac{(k_y^*)^2 V_0 V_n}{(\omega - k_y^* V_0) x_0 I_y} & \frac{(k_y^*)^2 V_0 V_n}{(\omega - k_y^* V_0) x_0 I_y} e^{-2k_y x_0} \end{bmatrix} \cdot \begin{bmatrix} A_1 \\ A_2 \end{bmatrix} = 0. \quad (\text{C5})$$

For ϕ_{DK}^{\sim} to be able to grow, this system of equations needs to have infinitely many solutions, implying that the determinant of the matrix in Eq. (C5) needs to be 0. This requirement restricts ω

$$\omega^2 = \left(\frac{k_y^* V_0 V_n}{k_y V_1 x_0 I_y} - 2k_y^* V_0 \right)^2 - \left(\frac{k_y^* V_0 V_n}{k_y V_1 x_0 I_y} \right)^2 e^{-4k_y x_0}. \quad (\text{C6})$$

For the instability to grow, we need $\omega^2 < 0$ which implies

$$\left(\frac{k_y^* V_0 V_n}{k_y V_1 x_0 I_y} - 2k_y^* V_0 \right)^2 < \left(\frac{k_y^* V_0 V_n}{k_y V_1 x_0 I_y} \right)^2 e^{-4k_y x_0}. \quad (\text{C7})$$

As can be seen, if V_n and V_1 have the same sign, this relation can only be satisfied for small $k_y x_0 < 1/4$ (necessary but not sufficient condition). In the limit $x_0 \rightarrow 0$, we get $1 > V_n/V_1 I_y$ and the instability condition in Eq. (8.3) is recovered. It is noted that this instability is limited by diffusion (numeric and physical through the collision operator) which restricts the development of small x_0 . Finally, the instability gives rise to more small-scale gradients in ϕ_{DK}^{\sim} which can drive a cascade of small-scale instabilities.